Atmospheric Structure and Composition,

D. F. Strobel, S. K. Atreya, B. Bézard, F. Ferri, F. M. Flasar, M. Fulchignoni, E. Lellouch , and I. Muller-Wodarg, in *Titan from Cassini-Huygens* (R.H. Brown et al., eds.), Chapter 10, pp 235-257, 2009, DOI 10.1007/978-1-4020-9215-2_10, Springer Dordrecht, Heidelberg-London-New York.

Chapter 10
Atmospheric Structure and Composition

Darrell F. Strobel, Sushil K. Atreya, Bruno Bézard, Francesca Ferri, F. Michael Flasar, Marcello Fulchignoni, Emmanuel Lellouch, and Ingo Müller-Wodarg

Abstract Titan's atmosphere is predominantly N_2 with CH_4 the next most abundant molecule. It has a mole fraction of 0.05 just above the surface decreasing to 0.014 in the stratosphere. Above the homopause (~800–850 km), it increases to 0.12 at the exobase. The third abundant molecule is H_2 with a tropospheric mole fraction of 0.001 increasing to 0.004 at ~1000 km and ~0.02 at the exobase (~1500–1600 km). This chapter reviews the various measurements acquired by the Voyager flybys, Huygens Probe, orbiting Cassini spacecraft, ground-based and orbiting telescopes of the large suite of hydrocarbons, nitriles, other nitrogen and also oxygen bearing compounds. Titan possesses a mostly stable troposphere with a well defined tropopause (T ~ 70 K at ~44 km) and a lower stratosphere with a high static stability, which is extremely cold over the winter polar region (currently northern hemisphere) and warm over the summer pole. Remarkably in the middle stratosphere, the warmest temperatures occur at the equator and the largest meridional temperature gradients are found in the winter hemisphere. The stratopause from the summer pole to about 45° N remains at a relatively constant pressure of 0.1 mbar/300 km and then it rises rapidly upward to ~0.01 mbar/400 km at the winter north pole, where it is the warmest region in the entire atmosphere. One possible interpretation of the Huygens Atmospheric Structure Instrument (HASI) temperature profile is that Titan's atmosphere is essentially isothermal ~170 K from 500–1100 km, with large amplitude thermal waves (10 K) superimposed. The existence and location of a well defined mesopause is an open question.

The chemistry of Titan's atmosphere is driven by CH_4 photolysis in the thermosphere and catalytic reactions in the stratosphere, and by N_2 dissociation due to both UV photons and energetic electrons. Ethane is the most abundant gas product and HCN is the dominant nitrile. The mixing ratios of all photochemical species, except C_2H_4, increase with altitude at equatorial and southern latitudes, indicative of transport from a high-altitude source to a condensation sink in the lower stratosphere. Northward of 45° N, most product compounds are enriched as a consequence of subsidence in the winter polar vortex, particularly for nitriles and more complex hydrocarbons than C_2H_6 and C_2H_2. North of 45° N, most products have lower increases with altitude than at low latitudes.

D.F. Strobel (✉)
The Johns Hopkins University, Baltimore, MD, 21218–2687, USA
e-mail: strobel@jhu.edu

S.K. Atreya
University of Michigan, Ann Arbor, MI, 48109–2143, USA
e-mail: atreya@umich.edu

B. Bézard, M. Fulchignoni and E. Lellouch
LESIA, Observatoire de Paris-Meudon, 92195, Meudon Cedex, France
e-mail: Bruno.Bezard@obspm.fr
e-mail: marcello.fulchignoni@obspm.fr
e-mail: emmanuel.lellouch@obspm.fr

F. Ferri
CISAS G.Colombo, University of Padova, 35131, Padova, Italy
e-mail: francesca.ferri@unipd.it

F. Michael Flasar
NASA Goddard Space Flight Center, Greenbelt, MD, 20771, USA
e-mail: f.m.flasar@nasa.gov

I. Müller-Wodarg
Space and Atmospheric Physics Group, Imperial College London, Prince Consort Road, London, SW7 2BW, UK
e-mail: i.mueller-wodarg@imperial.ac.uk

10.1 Historical Introduction

The first definitive detection of an atmosphere on Titan was Kuiper's (1944) discovery of near-IR CH_4 bands in absorption. But it was not until the 1970s, that Titan became an object of intense study. Lewis (1971) noted that Titan's low density implied an interior composition rich in ices and suggested photolysis of outgassed ammonia would lead to a nitrogen atmosphere. Trafton (1972) reported the possible detection of H_2 and interpreted the 20 μm spectral region in terms of a strong greenhouse. Gillett et al. (1973) detected pronounced peaks at 12 (C_2H_6) and 8 (CH_4) μm in narrow band spectra, which Danielson et al. (1973) interpreted as emission from a thermal inversion layer and substantial amounts of C_2H_6 (~3×10^{19} cm^{-2}) in the atmosphere. Two NASA Workshops and their reports (Hunten 1974; Hunten and Morrison 1978) enhanced

R.H. Brown et al. (eds.), *Titan from Cassini-Huygens*,

and focused the intense interest in Titan in anticipation of the Voyager flybys years later. Lewis' (1971) ideas for a nitrogen atmosphere from ammonia photolysis were pursued by Hunten (1978) and Atreya et al. (1978). The ambiguous (at the time) spectroscopic evidence on what are the major atmospheric species and surface pressure was interpreted by Hunten (1978) to imply a very thick background atmosphere (~20 bar of nitrogen) in addition to the observed CH_4. Danielson et al. (1973), in contrast, interpreted the spectroscopic evidence in terms of a very thin few mbar atmosphere of mostly CH_4. With these two divergent working models, the Voyager Missions' scientific objectives for Titan's atmosphere were well focused toward a definitive determination of its composition and structure. More pre-Voyager history and background may be found in the companion Chapter 2.

The Voyager spacecrafts yielded definitive measurements and answers to the outstanding questions at the time about Titan's atmosphere. The most noteworthy results were (1) composition, 97% N_2, except in the lowest 15 km, with 1.5–3% CH_4, <10% Ar, <5% CO (Broadfoot et al. 1981; Hanel et al. 1981; Strobel and Shemansky 1982; Strobel et al. 1993; Vervack et al. 2004), (2) the density, pressure, and temperature profiles at equatorial latitudes from the surface up to 200 km from the Voyager radio (refractive) occultation experiment (Lindal et al. 1983; Lellouch et al. 1989), (3) thermal and chemical structure from the Voyager IRIS Instrument at the surface, tropopause, and stratosphere at latitudes between 60º S to 70º N and detection of a large suite of hydrocarbons and nitriles in Titan's stratosphere (Hanel et al. 1981), and (4) the equatorial thermospheric structure from the Voyager Ultraviolet Spectrometer solar (absorptive) occultation experiment for N_2 and CH_4 between 900 and 1400 km (Broadfoot et al. 1981; Vervack et al. 2004). Additional Voyager background perspective can be found in Chapter 2.

The Cassini–Huygens Mission visited the Saturnian System some 20 years later with well-instrumented orbiting spacecraft and Huygens Probe, which descended to Titan's surface, to study in-depth Titan's atmosphere. In the following discussion the scientific discoveries and findings from this Mission on the structure and composition are reviewed and integrated with scientific knowledge derived from ground-based and orbiting observatories and Voyager.

10.2 Vertical Structure of the Atmosphere: Mass Density, Pressure, and Temperature

To understand the structure of Titan's atmosphere one must keep in mind certain basic facts from solar system dynamics (cf. Fig. 10.1). First, the axial tilt of Saturn and Titan is 26.73º and hence seasonal effects are important. Second, Saturn's orbital eccentricity is 0.05415, which yields a variation in the distance from the Sun of slightly greater than 1 AU and in the solar flux of ~20 %. Perihelion last occurred in 2003.56 and summer solstice in Titan's southern hemisphere was 2002.76, as shown in Fig. 10.1. The variation in solar distance and thus solar flux will be most important in the troposphere and stratosphere, whereas the much larger solar cycle variations in UV and EUV solar radiation will overwhelm the smaller eccentricity effects in the thermosphere. The Voyager spacecraft flybys were at high solar activity, whereas orbit insertion of the Cassini spacecraft in July 2004 was during the descending phase from peak activity, which occurred in April 2000, to solar minimum conditions in the August-November 2007 timeframe. Accordingly, the nominal Cassini–Huygens Mission was mostly at low solar activity.

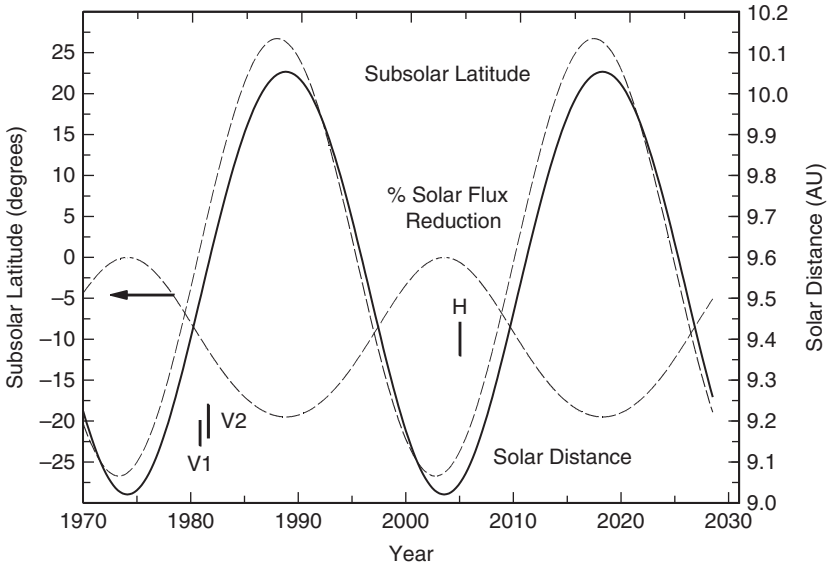

Fig. 10.1 The latitude of the subsolar point (dashed line), the distance from the Sun in AU (*solid line*), and the percentage variation in solar flux relative to perihelion as a function of time in years (*dashed line, read ordinate as %*). Last perihelion was 2003.56; last summer solstice in southern hemisphere was 2002.76. The Voyager flybys (V1, V2) and the Huygens Probe entry (H) are indicated

The most significant spatial variation in a planetary atmosphere is the vertical stratification due to gravity and characterized by an e-folding pressure scale height H, which for Titan varies from 15 to 100 km. As a consequence it is natural to take the distribution of the three thermodynamic variables that describe planetary atmospheres: mass (ρ) or number (n) density, pressure (p), and temperature (T) and write them, e. g. the latter as

$$T(\phi,\theta,z,t) = \langle T\rangle(z) + \overline{T}(\theta,z,t) + T'(\phi,\theta,z,t).$$

The first term is the vertical temperature profile with T averaged over the globe on each height or pressure surface if $z = -\int H(d\ln p)$, depending on the altitude variable. The second term is temperature departure from the first term averaged over longitude, ϕ, on a latitudinal circle at latitude θ and height z. The last term is the longitudinally varying departure from the first two terms and characterizes waves in the atmosphere. Seasonal variations are presumed to be present in the latter two quantities and absent from the first term in the troposphere and lower stratosphere, because of the long radiative time constants. Since most pronounced seasonal time variations are expected at high latitudes, 1D vertical profiles obtained at equatorial latitudes should be approximately equal to rigorously calculated $\langle T\rangle(z)$ from global data.

In Fig. 10.2, various 1D profiles obtained at equatorial latitudes are compared. For the Voyager radio occultation data acquired at 6.2ºN and 8.5ºS, the Lellouch et al. (1989) analysis is adopted. For the UVS solar occultation data taken at 4ºN and 16ºS, the Vervack et al. (2004) profile is shown and would imply T ~ 155 K atmosphere, if isothermal. From these data sets, the Yelle et al. (1997) engineering model was constructed for Cassini–Huygens Mission planning. Note that the agreement of this model with the Huygens Atmospheric Structure Instrument (HASI, Fulchignoni et al. 2005) density profile was excellent below 600 km. HASI measured entry deceleration from which density was derived directly down to an altitude of ~175 km, but pressure and temperature were inferred with the assumption of hydrostatic equilibrium. After ejection of the aeroshell and parachute deployment at z ~ 150–175 km, the pressure and temperature were independently measured and density derived from the equation of state for a real gas.

The lack of any change in Titan's lower atmosphere between the Voyager flybys and Huygens Probe is easily understood by the very long radiative time constants (~300 year at 10–20 km, ~60 year at 50 km) in comparison to a Saturnian year (= 29.5 year). In the thermosphere, the mass density measured by HASI is higher by up to a factor of 2 than inferred by Vervack et al. (2004) from the Voyager solar occultation measurements. The Voyager data were taken during solar maximum activity, whereas the HASI data were obtained when solar activity was between medium and minimum solar activity. Hence one would have expected Titan's upper atmosphere to have contracted relative to the Voyager epoch. Note that the Vervack et al. (2004) inferred temperature ~155 K, is about 20 K colder than HASI, so that extrapolating their densities to lower altitudes would merge with the HASI densities at ~1000 km. However due to Saturn's elliptical orbit around

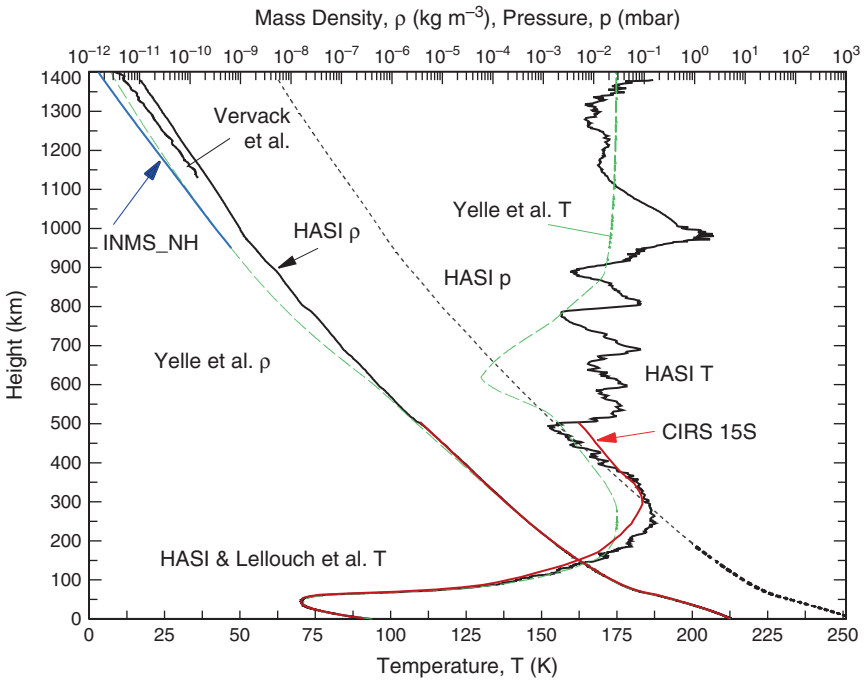

Fig. 10.2 Comparison of Cassini–Huygens HASI density, pressure, and temperature profiles (*black lines*, Fulchignoni et al. 2005), CIRS density and temperature profiles at 15 S (*red lines*, Vinatier et al. 2007a), average INMS Northern Hemisphere density profile (*blue line*, Müller-Wodarg et al. 2008) with the Voyager Lellouch et al. (1989) and Vervack et al. (2004) results, and the Yelle et al. (1997) engineering model (*green lines*), all as functions of altitude above surface

the Sun, Titan was at 9.44 AU during the Voyager 1 flyby and 9.04 AU, at the time of Huygens Probe entry. This could explain the expanded atmosphere, but not the colder temperatures in the thermosphere as the solar EUV and UV fluxes at solar maximum activity for Voyager flybys ratioed to solar fluxes pertinent to Probe descent would be ~2, more than enough to offset the $(9.44/9.04)^2$ ~1.09 factor due to Titan being closer to the Sun during the Probe descent. There is presently no explanation for the temperature difference between Vervack et al. and HASI.

Also shown in Fig. 10.2 is the Ion Neutral Mass Spectrometer (INMS) in situ data averaged for the northern hemisphere (Müller-Wodarg et al. 2008), which is about a factor of 2.4 lower than the HASI densities at 10.3° S. As discussed in more detail below and in Chapter 11, the drag and torque on the Cassini spacecraft allow determination of densities, which are systematically higher than measured INMS densities by a factor of ~2.6 on each pass through the upper atmosphere when INMS is making measurements of the neutral atmosphere. The drag determined densities from HASI support the Cassini spacecraft derived values.

With reference to Fig. 10.2, Titan possesses a well defined equatorial tropopause with T = 70.43 ± 0.25 K at 44 km. Based on the mean temperature profile the troposphere is statically stable. The low temperatures and high densities in the troposphere require that the atmosphere be treated as a real rather than an ideal gas. Titan's lower stratosphere has a high static stability with dT/dz ~1 K km^{-1}, from strong solar heating by its haze absorbing visible and UV radiation and near-IR CH_4 absorption (cf. Sec. 10.4.1). The stratopause according to HASI data is located at 260 km where T = 187 K. However, the CIRS stratospheric temperature retrievals do not agree with the HASI location and instead place it at ~312 km, where T = 183 K (Vinatier et al. 2007a). At this altitude, the HASI temperature is 184 K, but more important the CIRS temperature is 181 K at 265 km, and computation of the IR radiance with the HASI derived atmosphere is inconsistent with the observed CIRS CH_4 7.7 μm band radiance. In spite of these differences in temperature, there is remarkable agreement in mass densities up to 500 km, the upper boundary for CIRS retrievals.

Fulchignoni et al. (2005) identify the temperature minimum, 153 K at 494 km, as the Titan mesopause. The Yelle et al. (1997) engineering model required a well defined mesopause somewhere to satisfy Voyager data obtained in the lower/middle atmosphere and the thermosphere, but its location and minimum temperature were less constrained. Just above this HASI minimum is a pronounced temperature inversion with peak temperature of 169 K and temperature gradient of ~3.5 K km^{-1}. This feature was previously detected in stellar occultation measurements, (e. g., Sicardy et al. 2006) and is the location of a detached haze layer (Porco et al. 2005). Only a very small optical depth would suffice to absorb sufficient solar radiation to balance the implied substantial heat loss by thermal conduction (Lavvas et al. 2009).

The HASI temperature profile contains oscillations growing in amplitude above 200 km, which is consistent with propagating waves in a gas with exponential decreasing density, a possibility anticipated by Strobel and Sicardy (1997) in their engineering study. One possible interpretation of the HASI temperature profile is that Titan's atmosphere is essentially isothermal ~170 K from 500–1100 km, with large amplitude thermal waves (10 K) superimposed on an isothermal basic state. Calculation of the wave temperature lapse rate (dT/dz) yields values that exceed the adiabatic lapse rate (= g/c_p, which varies from 1.24 at the surface to 0.56 K km^{-1} at 1400 km) at multiple altitudes throughout the atmosphere with the conclusion that the waves attain breaking/saturation amplitudes (cf. Fig. 3 in Fulchignoni et al. 2005). The large vertical wavelengths associated with the largest amplitudes imply either strong horizontal winds and/or high phase speeds for propagating waves.

The mean temperature profile above 1000 km does not have to be isothermal. Strobel (2008) has theorized that the large escape rates deduced from Cassini INMS data for CH_4 and H_2 (Yelle et al. 2008; Cui et al. 2008) can be explained by slow hydrodynamic escape, with no requirement for large non-thermal escape. The bulk outflow produces adiabatic cooling and approximately $T \propto r^{-1}$. Superposition of waves on this slowly decreasing mean temperature profile could also account for the derived HASI temperature (and density) data above ~1000 km. Potential wave sources are gravitational tides, large wind shear creating Kelvin–Helmholtz instability, and gravity waves forced by topography. Further discussion on wave dynamics of the atmosphere is found in Chapter 13.

10.3 The Height and Latitude Structure of the Atmosphere

Below the relevant Cassini observations performed during the nominal mission (RSS radio occultations, CIRS remote sensing, UVIS solar and stellar occultations, and INMS in situ measurements) are discussed with an emphasis on the height and latitude variations of density, pressure, and temperature.

10.3.1 Radio Occultations

There was only one Titan earth occultation of the Voyager spacecraft (Vgr 1), with ingress at 6°N and egress at 9°S. The retrieved temperatures were nearly identical in the troposphere, with a lapse rate close to the dry adiabat in the

lowest 3–4 km. Cassini had four occultations by Titan, with ingress and egress soundings at 74°S, 69°S, 53°S, 34°S, 33°S, 32°S, 53°N, 74°N. Although the data have not been fully analyzed, the occultations agree with the Voyager IRIS observations in indicating a small meridional variation of temperature in the troposphere. At the tropopause, temperatures retrieved from the occultations vary by 4–5 K. Near the surface they differ by ~3 K or less. The coldest temperatures are at higher northern latitudes. Temperature profiles near 30°S are nearly adiabatic above the surface. At higher latitudes they become more stably stratified above the surface and in the winter, northern latitudes, temperatures are isothermal or have an inversion above the surface. Data for the lower northern polar stratosphere is of particular interest, because accurate retrievals from CIRS far-IR limb soundings are exceedingly difficult and there is no information from CIRS mid-IR soundings of the polar lower stratosphere as it is too cold.

10.3.2 Remote Sensing

In Fig. 10.3, the temperature of Titan's stratosphere and mesosphere is displayed as a function of latitude (75º S to 75º N) and pressure (0.001 to 10 mbar) and based on CIRS data acquired over the period from July 2004 to September 2006 (Achterberg et al. 2008). Referring to Fig. 10.1, this period is mostly solstitial. While no altitude scale is shown, one can refer to Fig. 10.2 and use the altitude scale for the CIRS 15S profile, which should be reasonable for latitudes spanning 65º S to 30º N. Remarkably in the stratosphere, the warmest temperatures occur at the equator and the largest meridional temperature gradients are found in the winter (currently, northern) hemisphere rather than in the summer (southern) hemisphere. The other noteworthy feature is the extremely cold lower polar stratosphere in the northern winter hemisphere, where the temperatures decrease by ~25–30 K from 30º N to 75º N on constant pressure surfaces between 1 and 10 mbar. The stratopause remains at a relatively constant altitude and pressure of 300 km and 0.1 mbar, respectively from the summer pole to about 45º N, and then it rises rapidly upward to ~400 km at the winter north pole. In fact, the warmest region in the entire atmosphere is the winter, northern polar "stratopause" at ~0.01 mbar/400 km and about 20 K warmer than the equatorial and summer, southern regions. The polar night only extends to 315 km, so it's possible that this warm region may have a diabatic origin. However, the enhanced mixing ratios of nitriles and hydrocarbons at winter, northern polar latitudes (cf. Fig. 10.10) suggests that subsidence and adiabatic heating is certainly occurring.

At 19 μm, CIRS detects thermal radiation from the surface because the atmospheric opacity is small and the latitudinal variation of surface temperature can be inferred from brightness temperatures. Jennings et al. (2009) find that the north pole surface is 3 K lower and the south pole surface 2 K lower than the equatorial surface temperature of 93.7 ± 0.6 K, equal to the HASI value at 10º S.

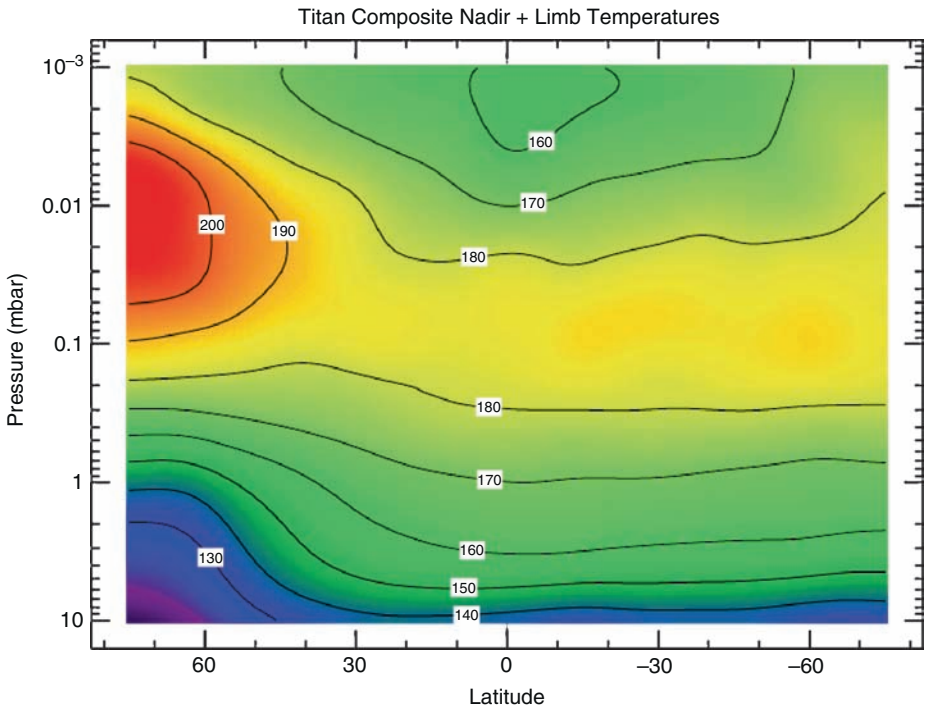

Fig. 10.3 CIRS zonal mean temperatures (K) from limb and nadir spectra recorded between July 2004 and September 2006. Retrieved temperatures were averaged over 5° latitudinal intervals and smoothed three times with 10° boxcar function (after Achterberg et al. (2008))

While HASI and refractive stellar occultations (discussed below) have detected wave structure in the atmosphere, CIRS has not to date and can only place an upper limit on wave temperature amplitudes of ~1 K. But it must be kept in mind that CIRS can only probe the atmosphere up to ~500 km, and then in the limb mode. The total data coverage of the atmosphere to date is limited in extent and it is possible that waves may be detectable by CIRS eventually. However, it is necessary to average CIRS spectra with a consequent loss of spatial resolution.

10.3.3 Solar and Stellar Occultations

The Voyager UVS solar occultations were equatorial and provided the extraordinary measurement that CH_4 was well mixed up to at least 1000 km (Vervack et al. 2004), since confirmed by the INMS (Waite et al. 2005; Yelle et al. 2008). The Cassini Ultraviolet Imaging Spectrometer (UVIS) has performed two solar occultations during the nominal mission, but no published reports are available on the results. Shemansky et al. (2005) have reported on the first UVIS stellar occultations. Their inferred temperature profile above 400 km contains (1) a convective region around 450 km where the temperature gradient is adiabatic and (2) a mesopause at 615 km with T = 114 K. By comparison, the HASI temperature was ~175 K there. When the UVIS retrieved temperature profile is used with the hydrostatic equation and lower boundary condition at 400 km from CIRS and HASI data to calculate the N_2 density profile, one obtains at 1200 km an N_2 density that is a factor of ~8 and ~20 times lower than measured by INMS and HASI, respectively. Also the UVIS inferred CH_4 densities at 1200 km when coupled with this calculated N_2 density implies that CH_4/N_2 ratio is ~0.5, also at variance with INMS values of ~0.035 at 1200 km. The INMS mixing ratios for major species should be far more accurate than absolute values of individual densities. Note that interstellar hydrogen ionizes and cuts off the stellar UV flux below 91.1 nm. Above this wavelength N_2 UV absorption occurs only in predissociated electronic bands that are very difficult to interpret at UVIS spectral resolution.

Beside absorptive occultations, there have been a few refractive stellar occultations (July 1989; 21 August 1995; 20 December 2001; two on 14 November 2003) mostly at visible wavelengths. These occultations were measured with ground-based telescopes, while the previously discussed ones were measured by onboard Cassini instruments. For the November 2003 events as representative, Sicardy et al. (2006) probed the 0.1–250 μbar region of Titan's atmosphere. However, the 0.1–1 μbar region is subject to initial conditions in their onion peeling analysis procedure and for pressures greater than 12 μbar (400 km), the stellar fluxes are attenuated by haze absorption in addition to the usual refraction effects. The retrieved temperature profile is in essential agreement with the HASI temperature profile and, in particular, the presence of abundant wave signatures and temperature gradients that exceed the adiabatic lapse rate. As noted above, there is a pronounced thermal inversion layer at 1.5 μbar (~507–515 km). From the central flash analysis which extracts latitudinal information, Sicardy et al. (2006) found an isopycnic surface equal to approximately the 250 μbar surface which rises about 50 km in altitude above an arbitrary north pole reference height when 45° N is reached and remains relatively constant all the way to the south pole. This is consistent with very strong stratospheric zonal winds in the winter northern hemisphere and much weaker zonal winds in the summer hemisphere, as found by CIRS (Achterberg et al. 2008)

10.3.4 In Situ Measurements

The first in-situ measurements of Titan's upper atmosphere were carried out by the Cassini INMS during the first targeted Titan flyby (TA) on 26 October 2004. This initial dataset has been considerably expanded with subsequent targeted flybys, of which a total of 19 offered the INMS adequate observing conditions and produced data of sufficient quality. The INMS measured gas densities during 13 flybys primarily in the northern hemisphere and during the remaining 6 flybys in the southern hemisphere. Altitudes of closest approach ranged from 950 km (T16) to 1175 km (TA). The INMS can measure either in the Closed Source Neutral (CSN) or Open Source Ion (OSI) mode to retrieve neutral or ion densities, respectively. Ion composition was measured only during 9 of the 19 flybys and neutral densities during all, though not always on both inbound and outbound parts of the flybys.

Using the neutral gas density measurements of N_2 and CH_4 in the northern hemisphere, Müller-Wodarg et al. (2008) constructed a simple empirical model of gas densities and temperatures in the northern hemisphere based on flybys TA-T32. During these flybys the solar declination angle on Titan changed from -23° to -11°, so the season was in transition between southern hemisphere summer conditions and equinox. The model by Müller-Wodarg et al. (2008) can hence be regarded as an average representation of Titan's winter hemisphere. The vertical range is from 1000 to 1600 km, covering altitudes that were sufficiently sampled by the INMS. In their statistical analysis of the INMS N_2 and CH_4 densities, Müller-Wodarg et al. (2008) found no consistent trends with longitude or local time, which however may partly be due to uneven sampling which favored polar nightside or

low latitude dayside measurements, primarily in Titan's Saturn-facing longitude sector (Cui et al., 2008). A clear latitudinal trend was detected in the INMS densities at fixed height levels above around 1100 km (Fig. 10.4), with densities increasing towards the equator by around 70%. The density model was used to infer thermospheric temperatures in Fig. 10.4 which decrease with height from 149 ± 10 K at 1000 km to 140 ± 13 K near 1600 km, and with latitude below 1200 km with values near 1000 km from 164 ± 6 K at 20°N to 131 ± 6 K near 80°N.

While in-situ observations by the INMS have been made in the southern hemisphere during 9 passes, the statistical variation between these has been too large to derive a consistent latitudinal trend. Preliminary analysis of the structure of the southern hemisphere suggests temperatures to be warmer by ~10–15 K there than average values in the northern hemisphere, as expected from solar heating.

While the INMS has provided the most comprehensive set of observations yet in Titan's thermosphere, one uncertainty remains in the absolute calibration of densities. Comparison of INMS densities with those by the HASI observations at equatorial latitudes near 1000 km latitude shows INMS values to be 2.4 times smaller than the HASI values. The Cassini Attitude and Atriculation Control Subsystem (AACS) detects torques on the spacecraft as it enters Titan's upper atmosphere on each flyby, providing an additional independent measurement of total density. Comparison of AACS-derived densities at 1000 km and those from the INMS show INMS densities to again be smaller by an average factor of 2.6 than those from the AACS, very similar to the discrepancy factor between HASI and INMS at that altitude. This unresolved discrepancy however does not affect the inferred temperatures.

10.4 Interpretation of Atmospheric Temperature Structure

10.4.1 *Radiative Budget of Troposphere and Stratosphere*

Solar energy is absorbed in Titan's atmosphere through methane and haze absorption and at the surface. The Descent Imager/Spectral Radiometer (DISR) aboard the Huygens probe measured the downward and upward fluxes of sunlight at wavelengths from 350 to 1600 nm and altitudes from 150 to 0 km. These measurements have been analyzed to derive the vertical distribution and optical properties of haze aerosols (see Chapter 12), the absorption coefficients of methane in Titan's conditions, and the solar energy deposition profile at the latitude of the Huygens landing (10°S) (Tomasko et al. 2008). Averaged over a Titan day at the location and season of the Huygens landing, about 78% of the incoming sunlight is overall absorbed: ~11% at the surface, ~48% in the atmosphere below 150 km and ~19% above. The disk-averaged solar flux profile, calculated with the Huygens haze model, is shown in Fig. 10.5. It is in remarkable agreement with the earlier estimate of McKay et al. (1989) based on ground-based albedo and Voyager data.

Radiative cooling of the atmosphere occurs through thermal emission by haze particles and gases beyond ~7 μm (molecular bands and collision-induced opacity). Tomasko et al. (2008) calculated the radiative cooling rate profile at latitudes and time close to the Huygens landing using Cassini/CIRS nadir and limb measurements. As shown in Fig. 10.5, collision-induced opacity is the main source of atmospheric cooling below 80 km while, above, molecular

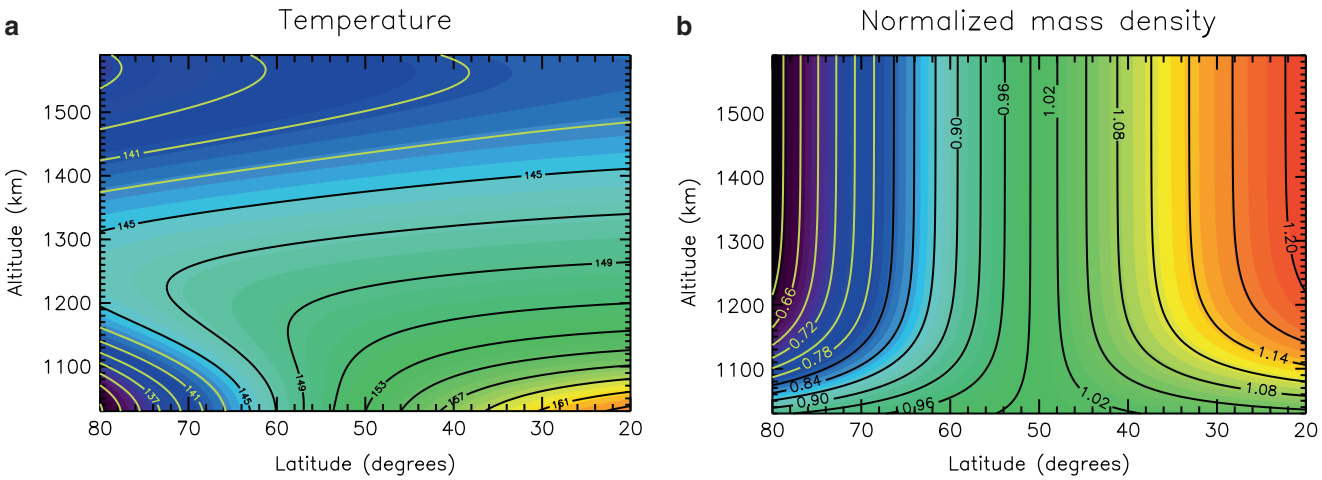

Fig. 10.4 (**a**) Temperatures in Titan's thermosphere inferred from an empirical model of atmosphere densities measured by INMS in the Northern Hemisphere. While the atmosphere is nearly isothermal above around 1200 km altitude, temperatures below 1100 km increase towards the equator. (**b**) Normalized Mass Densities at each height to the value at 50N from the empirical model. Note the bulge at the equator (after Müller-Wodarg et al. (2008))

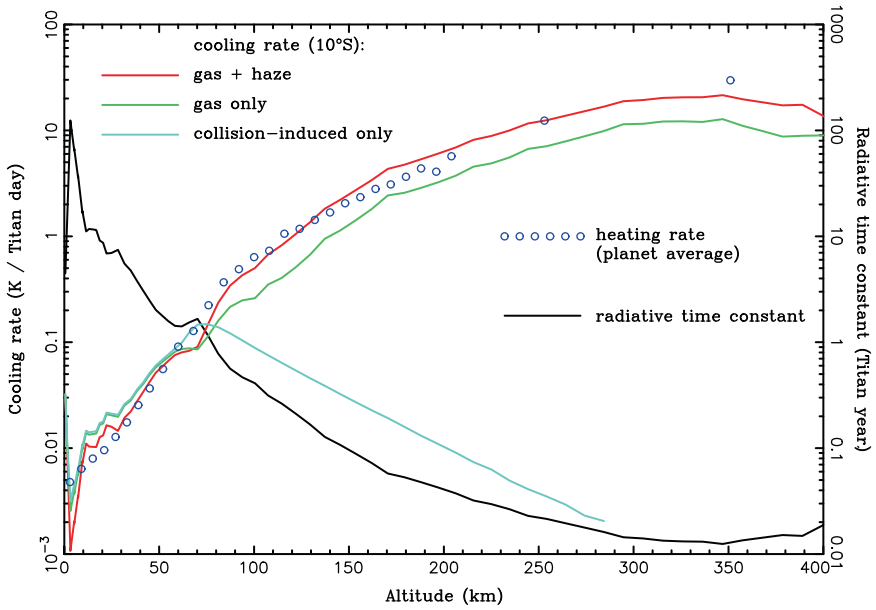

Fig. 10.5 Cooling rate profiles calculated around 10°S from Cassini/CIRS and Huygens data are compared with the solar heating rate profile, averaged over the planet, calculated from Huygens/DISR measurements (Tomasko et al. 2008). Cooling rates are best constrained in the ranges 10–65 km and 90–400 km and heating rates below 200 km. The radiative time constant (defined here as the temperature divided by the cooling rate) is also shown (*right y-scale*)

band and haze opacities dominate and are of comparable importance. The cooling rate reaches 10–20 K per Titan day at altitudes 250–400 km and decreases rapidly at lower levels. Dividing the temperature by the cooling rate provides a radiative time constant, also displayed in Fig. 10.5. It is short in the upper stratosphere and mesosphere (~0.5 Earth year, i.e. 0.015 Titan year, in the range 300–400 km), reaches a Titan year (29.5 Earth years) around 80 km, and is about 10 Titan years at 20 km. The cooling rate profile is close to that determined by Bézard et al. (1995) at 53°S from Voyager data at northern spring equinox. In the region best constrained by the Voyager/IRIS measurements (140–250 km), the two profiles agree within 20%.

The CIRS-derived cooling rate profile around 10°S is very close to the *disk-averaged* heating rate profile based on the Huygens haze model. Both decrease by three orders of magnitude from 350 to 10 km and agree at all levels within 50%. On the other hand, the solar heating rate at 10°S exceeds the cooling rate at all altitudes below 160 km, with a maximum net heating of about 0.5 K per Titan day located around 120 km. The general circulation likely redistributes this excess heat to higher latitudes.

Bézard et al. (1995) have shown that the latitudinal variations of composition strongly affect the radiative forcing in the stratosphere. At 50°N, the cooling rates derived from Voyager in the range 120–270 km (5–0.15 mbar) were some 20–40% larger than at 53°S despite the colder temperatures (7 to 15 K), a consequence of larger concentrations of infrared emitters (gas and particles). But, as the heating rate was also larger, radiative balance was still approximately achieved at this location within error bars. Using a general circulation model, Lebonnois et al. (2003b) also pointed out the strong enhancement of radiative cooling at high winter latitudes induced by the larger concentrations of some gases (C_2H_6, C_2H_2 and HCN). This thermal effect was found similar to that due to the coupling between aerosols and the general circulation (Rannou et al. 2002) in the mesosphere but smaller in the stratosphere around 1 mbar (190 km).

10.4.2 Radiative Processes in the Upper Atmosphere

Above 400 km (~0.03 mbar) non-LTE effects become important for hydrocarbon cooling rates as shown by Yelle (1991). Above 700 km (~0.1 μbar) he showed that HCN LTE rotational line cooling dominates radiative cooling to the exobase. The dominant heating processes above 400 km are near-IR CH_4 heating by absorption of solar radiation in the 1.7, 2.3, and 3.3 μm bands. Above ~650 km solar UV CH_4 heating emerges as the principal heat source and above 900 km, the thermosphere is, to zeroth order, in radiative equilibrium where solar EUV/UV heating is balanced by HCN rotational line cooling (Yelle 1991). Without HCN cooling calculated thermospheric temperatures would far exceed the observed values.

Yelle's models consistently predicted a pronounced mesopause at 600 km (~0.5 μbar) with ~25 K temperature drop from the 300 km temperature, whereas HASI data suggested the mesopause is at 494 km (Fulchignoni et al. 2005) with a temperature minimum of 153 K to be compared with ~185 K at 300 km. In Fig. 10.2 the Yelle et al. engineering model is representative of Yelle (1991) models and can be compared

with the HASI profiles. As noted above the steep temperature gradient in the HASI temperature profile above 494 km and inferred by Sicardy et al. (2006) from stellar occultations requires solar heating of the detached haze layer detected by Porco et al. (2005). Above this haze layer, Liang et al. (2007b) present evidence that the aerosols extend up to 1000 km. Heating associated with discreet haze layers and the broad distribution of aerosols above the visible disk of Titan were not included in the Yelle (1991) model, but were included in Lavvas et al. (2009), who used the Yelle computer code and found that the net effect was to raise the mesopause by ~50 km without changing its temperature, in farther disagreement with the HASI inferred mesopause at 494 km.

10.5 Composition

This section emphasizes the observational facts and divides the composition into four major categories. The major constituents, N_2, CH_4, H_2, and the inert, noble gases all have long chemical time constants and hence are expected to be well mixed throughout the homosphere, which extends from the surface to about 800–850 km (Yelle et al. 2008). The one exception to being well-mixed is CH_4, which is condensable in the troposphere. Minor constituents are subdivided into three main classes: pure hydrocarbons, nitriles, and molecules containing oxygen.

10.5.1 Major Constituents and Inert, Noble Gases

From the Voyager Mission, the major constituents of the atmosphere were known. But there was considerably uncertainty in the CH_4 mixing ratio: its variation in the troposphere, its magnitude in the stratosphere, and whether the tropopause region was an effective cold trap. The Huygens Gas Chromatograph Mass Spectrometer (GCMS) provided definite answers to these questions (Niemann et al. 2005). The tropospheric CH_4 mixing ratio (mole fraction) is variable with a maximum value just above the surface of 0.0492 and decreases gradually to initially an asymptotic value of 0.0162 at 32 km, and then more slowly to its measured stratospheric value of 0.0141 as shown in Fig. 10.6. In addition to GCMS, the Huygens Descent Imager/Spectral Radiometer (DISR) measured the surface CH_4 mixing ratio by near-IR spectroscopy to be 0.051 ± 0.008, in agreement with GCMS (Jacquemart et al. 2008). The CIRS inferred stratospheric value of 0.016 ± 0.005 (Flasar et al. 2005) is consistent with the in situ measurement.

The third most abundant species is H_2, for which GCMS has not reported a value. From the Voyager IRIS measurements the H_2 inferred mixing ratio was 0.00112 ± 0.00016 by Samuelson et al. (1997) and 0.001 ± 0.0004 by Courtin et al. (1995). CIRS measurements yield the same mixing ratio: 0.00096 ± 0.00024 southward of 40º N (Courtin et al. 2008). These values are appropriate for the troposphere/tropopause region. At very high altitudes INMS finds the H_2 mixing ratio to be 0.00405 ± 0.00003 (Waite et al. 2005). Given the large separation distance (~1000 km) between these two independent measurements, the factor of 4 difference would not seem significant except that H_2 tends to be essentially uniformly mixed throughout the atmosphere due to its long chemical lifetime and its enormous escape rate out of the atmosphere (1.1×10^{28} s^{-1}, Cui et al.; 2008) which is essentially equal to the maximum possible rate. This small positive gradient in the H_2 mixing ratio is not produced in photochemical models to date and remains a challenge to modelers.

The ^{40}Ar isotope is an important tracer used to determine vertical mixing in the atmosphere and the location of the homopause (cf. Yelle et al. 2008). The measured tropospheric mixing ratio by Huygens GCMS is (4.32 ± 0.1) × 10^{-5}

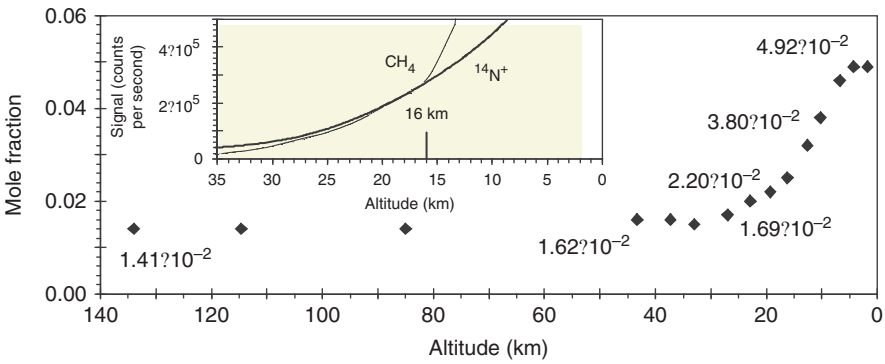

Fig. 10.6 The mole fraction of CH_4 to N_2 versus altitude. The CH4 mole fraction is 0.0141 in the stratosphere., at ~8 km, it reached a plateau of about 0.049. The inset shows an increase of CH_4 at 16 m/z, when compared to N_2 (in this case $^{14}N^+$) at m/z = 14, near 16 km. This is probably due to condensates evaporating in the inlet system of the mass spectrometer as the Huygens probe passed through the methane haze (after Niemann et al. (2005))

(Niemann et al. 2005), whereas in the thermosphere INMS measured $(7.1 \pm 0.1) \times 10^{-6}$ (Waite et al. 2005). Primordial ^{36}Ar is much less abundant, only $(2.8 \pm 0.3) \times 10^{-7}$ (Niemann et al. 2005). Other noble gases, Ne, Kr, and Xe, were not detected by the Huygens GCMS. The Huygens GCMS placed an upper limit of 10^{-8} on Kr and Xe, well below their cosmogonic abundance, as was also the very low, constraining value for ^{36}Ar. The $^{14}N/^{15}N$ isotope ratio measured in situ in N_2 by the GCMS (183; Niemann et al. 2005) is a factor three larger than that inferred from HCN (Vinatier et al. 2007b). The implications of these isotopes for the evolution of Titan's nitrogen atmosphere are discussed in detail in Chapter 7.

10.5.2 Minor Constituents – Hydrocarbons Other than Methane

Voyager/IRIS observed a suite of hydrocarbons produced from methane photochemistry and mapped their abundances in the lower stratosphere between 50°S and 70°N (Coustenis and Bézard 1995). Cassini/CIRS improved over the IRIS observations thanks to a higher spectral resolution (up to 0.5 cm^{-1}), a broader spectral range (10–1500 cm^{-1}), the use of limb-viewing geometry, and a much more extended spatial and temporal coverage (Fig. 10.7). Nadir measurements provide information on the mean gas abundances in a broad region usually centered around 120 km while limb-viewing measurements probe the atmosphere up to ~500 km.

The hydrocarbon mixing ratios in the lower stratosphere have been derived by Coustenis and Bézard (1995), Flasar et al. (2005), and Coustenis et al. (2007) from IRIS and CIRS nadir spectra respectively (Fig. 10.8). Ethane (C_2H_6) is the most abundant photochemical product (~10 ppm at 120 km), followed by acetylene (C_2H_2), propane (C_3H_8), ethylene (C_2H_4), methyl acetylene (CH_3C_2H), diacetylene (C_4H_2) and benzene (C_6H_6, which was not detected in IRIS spectra). The mixing ratio decreases with the complexity of the molecule as would be expected and, for a given number of C-atoms, saturated species are more abundant that unsaturated ones. All hydrocarbons are more abundant northward of 45°N. This enrichment is larger for C_4H_2 and CH_3C_2H than for the more stable species C_2H_6 and C_2H_2. It is more pronounced in the Voyager data recorded in 1980, a season close to northern spring equinox, than observed by Cassini in 2005 shortly after winter solstice (Figs. 10.1 and 10.8). In contrast, images taken in the period 1999–2002 with the Keck telescope at 8–13 μm suggest an accumulation of C_2H_4 in the polar stratosphere south of 60°S (Roe et al. 2004). If real, this polar enhancement, persisting through late southern Spring, has rapidly disappeared as it was not seen by Cassini three years later, i.e. one tenth of a Titan year later.

Vertical profiles have been inferred from two CIRS sequences combining nadir and limb spectra at 15°S and 80°N (Vinatier et al. 2007a) and subsequently at other latitudes (Vinatier 2007; Teanby et al. 2008b). Information is available from about 500 km down to 100–150 km. At southern and mid northern latitudes, all mixing ratio profiles, except ethylene, increase with height (Fig. 10.9). This results

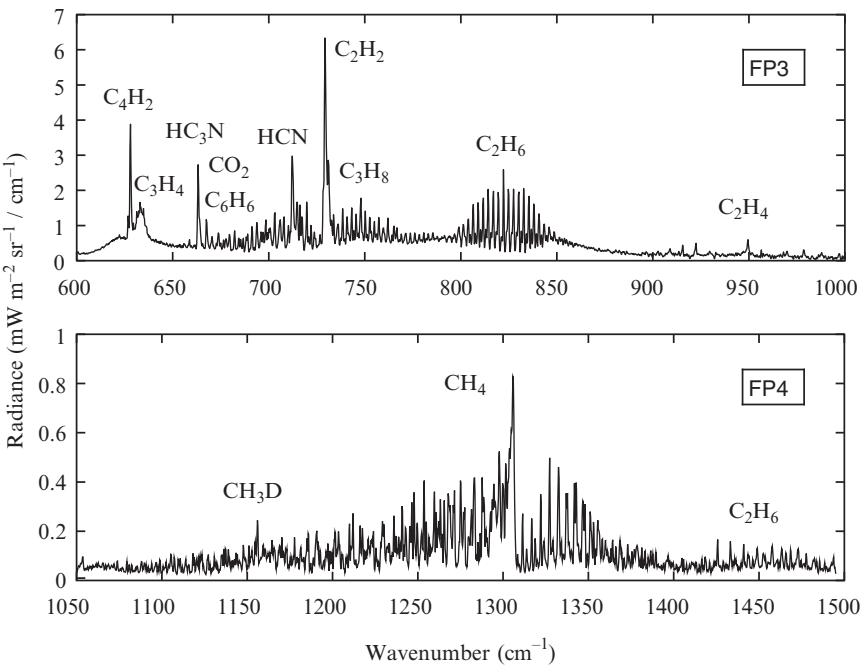

Fig. 10.7 An average of Cassini/CIRS limb spectra recorded at 100–200 km altitude and high northern latitudes, showing emission features from various hydrocarbons and nitriles. To analyze the observations, the temperature profile is first retrieved from the 1305 cm^{-1} (7.7 μm) methane band and the gas mixing ratio profiles are derived from the corresponding emission bands (from Bézard 2009))

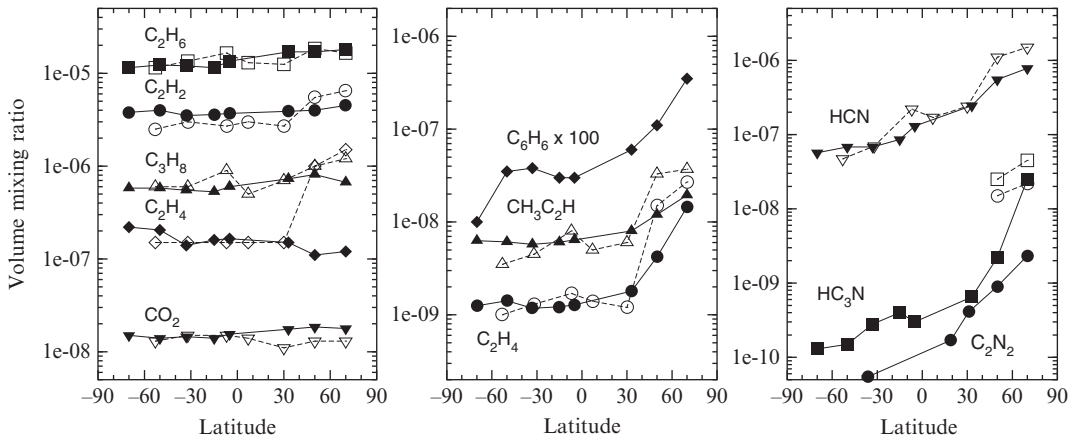

Fig. 10.8 Meridional variation of composition in the lower stratosphere around 120 km. Filled symbols and solid lines represent data from Cassini/CIRS spectra in 2005. Empty symbols and dashed lines correspond to mixing ratios derived by Voyager 1 in November 1980 (from Bézard 2009)

from photochemical production in the upper atmosphere (>500 km) and loss by condensation in the lower stratosphere (60 to 100 km depending on the species), which together maintain a positive concentration gradient. This gradient is moderate for C_2H_6 and C_2H_2 and steepest for C_4H_2 which undergoes chemical losses in the stratosphere (see Fig. 10.9). Ethylene is the only species whose mixing ratio decreases with height between 120 and 250 km, a behavior that may result from the fact that it does not condense and can be enriched in the lower atmosphere by equatorward transport of polar air (Crespin et al. 2008). At high northern latitudes, beyond 45°N, the vertical profiles change drastically and exhibit larger concentrations in the lower stratosphere at least below 250–300 km (Figs. 10.9 and 10.10). At 50–60°N, concentration minima are seen at 350–400 km for C_4H_2 and C_2H_2. These minima also exist at ~80°N but seem to occur at somewhat lower altitudes (~300 km) and be less pronounced. At this latitude (80°N), minima are also observed for CH_3C_2H, C_2H_4 and C_2H_6 as shown in Fig. 10.9. A similar pattern exists for nitriles and likely results from dynamical processes associated with the polar vortex as discussed in Sec. 10.5.3. Little is known on the vertical profile of benzene, the least abundant hydrocarbon detected: at 79°N, its mixing ratio is constant within error bars (3–4 ppb) between 180 and 320 km (Vinatier 2007), i.e. about 10 times larger than at mid-latitudes and ~120 km (Coustenis et al. 2007).

Above 500 km, the atmospheric composition can be probed by stellar or solar occultations observed from spacecraft. A reanalysis of the Voyager 1 UVS solar occultations at latitudes of 4°N (ingress) and 16°S (egress) provided density profiles of two hydrocarbons besides methane: C_2H_2 and C_2H_4 (Vervack et al. 2004). The C_2H_2 mixing ratio agrees very well with that derived from Cassini/CIRS at 15°S (Fig. 10.9) while the C_2H_4 value is about 2 orders of magnitude larger than the CIRS value at 240 km, suggesting that a minimum exists in its mixing ratio profile somewhere between 250 and ~450 km. Above 500 km, the mixing ratios of C_2H_2 and C_2H_4 increase with height to reach respectively (0.6–2) × 10^{-3} and (0.3–2) × 10^{-3} at 950 km, pointing to a source at higher altitudes. A stellar occultation observed by Cassini/UVIS at 36°S provided density profiles of several hydrocarbons between ~1000 km and a lower limit ranging from 615 to 845 km (Shemansky et al. 2005). The C_2H_4 number densities inferred between 845 and 1000 km agree within error bars with those from Voyager 1 UVS. On the other hand, the C_2H_2 number density at 615 km is about 20 times larger than the UVS value at the same altitude and the corresponding mixing ratio (assuming a CH_4 mole fraction of 0.014) is about 50 times larger than the CIRS value at 500 km, which casts doubts on the reported UVIS results.

At higher altitudes, the composition of the thermosphere and ionosphere has been probed in situ by the INMS aboard Cassini. During the first low-altitude pass through Titan's atmosphere at ~39°N latitude (Ta), INMS detected the neutrals C_2H_2, C_2H_4, C_2H_6, C_3H_4, C_4H_2 and C_6H_6 around 1200 km. Benzene has been detected by INMS in many passes through Titan's atmosphere. An analysis of the signals recorded during T16 indicates a mole fraction of 1.3 × 10^{-6} at 950 km near the North Pole (Vuitton et al. 2008). This implies an ionospheric source of about 10^7 molecules cm^{-2} s^{-1}, of the same magnitude as the neutral production rate in the stratosphere needed to explain the CIRS abundance. Measurements of ion densities coupled with simple chemical models provide an additional probe of the composition of the neutral atmosphere. This allowed the detection of C_2H_4, polyynes (C_4H_2, C_6H_2, C_8H_2) and possibly methylpolyynes (CH_3C_4H, CH_3C_6H) and a determination of their mole fractions around 1100 km at 74°N during the T5 flyby (Vuitton et al. 2006, 2007). A review of the composition of Titan's thermosphere and ionosphere can be found in Chapter 11.

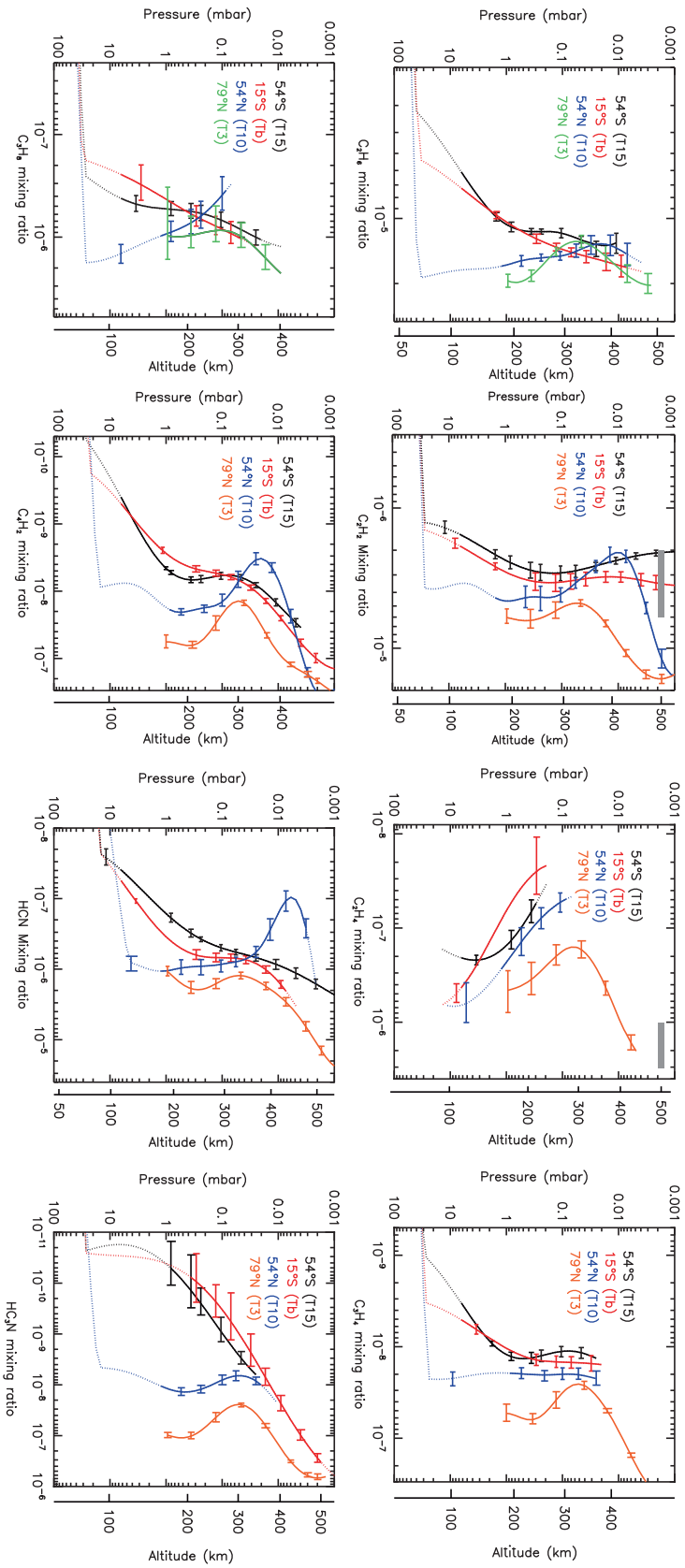

Fig. 10.9 Vertical profiles of hydrocarbons and nitriles obtained from inversion of Cassini/CIRS nadir and limb spectra recorded at four latitudes (54°S, 15°S, 54°N, and 79°N). The error bars are indicated at the maxima of the inversion kernels, which is the level of maximum information in the spectral sequences analyzed. The thick grey segment represents the Voyager 1 UVS measurement at 4°N (adapted from Vinatier 2007)

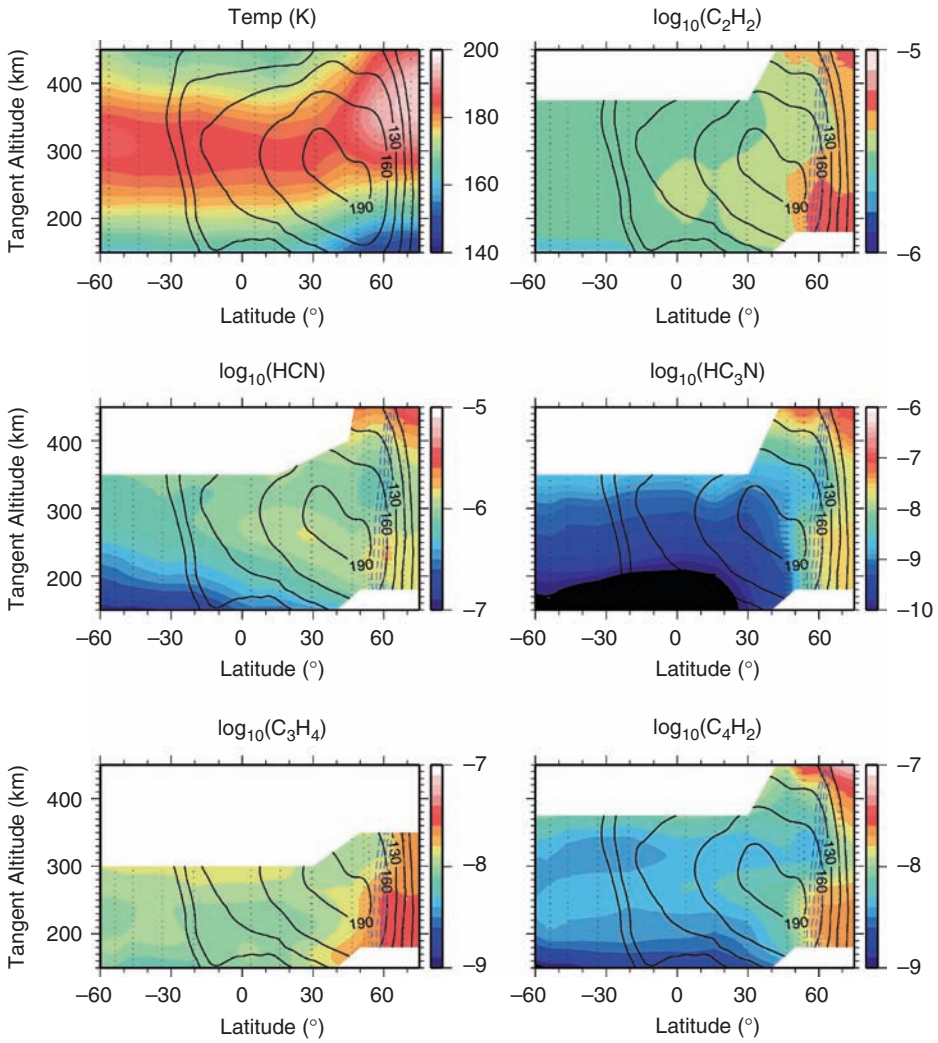

Fig. 10.10 Cross sections of temperature and composition through Titan's atmosphere constructed from Cassini/CIRS observations in 2006–2007. Composition is given as a volume mixing ratio and the position of the observed profiles are denoted by dotted lines. Contours indicate the vortex zonal wind speeds (in m s^{-1}) and blue dashed lines show the region with the steepest horizontal potential vorticity gradient, which indicates a dynamical mixing barrier (from Teanby et al. 2008)

10.5.3 Minor Constituents – N-Bearing Species and Nitriles

Voyager/IRIS and Cassini/CIRS detected three nitriles in Titan's stratosphere: hydrogen cyanide (HCN), cyanoacetylene (HC_3N) and cyanogen (C_2N_2) (Coustenis and Bézard 1995; Teanby et al. 2006). Mixing ratios derived from nadir spectra are shown in Fig. 10.8 as a function of latitude, assuming uniform profiles above the condensation levels. HCN, the simplest and most abundant nitrile, is detected at all latitudes. Its mixing ratio is fairly constant southward of 20°S (~1 × 10^{-7} around 150 km) and gradually increases towards the north. The north-to-south asymmetry is more dramatic for the two other species. In particular, the C_2N_2 signature is extremely weak in CIRS spectra of the southern hemisphere and equatorial region and indicates a mixing ratio as low as 6 × 10^{-11} (Teanby et al. 2009). On the other hand, it is clearly detected at high northern latitudes with a mixing ratio of 9 × 10^{-10} at 50°N and around 3 × 10^{-9} beyond 70°N. As for hydrocarbons, the enhancement of nitriles north of ~45°N was more pronounced at the Voyager encounter time than at the beginning of the Cassini mission.

Vertical profiles of HCN and HC_3N have been derived using CIRS limb observational sequences in the range 100–500 km at a variety of latitudes (Teanby et al. 2007; Vinatier 2007). From southern to mid-northern latitudes (<40°N), the HCN mole fraction increases regularly with height (by a factor of ~30 from 100 to 400 km) while HC_3N exhibits a much steeper gradient, increasing by at least 3 orders of magnitude between 200 and 500 km. The HC_3N profile is consistent with those derived from ground-based millimeter and submillimeter heterodyne observations (Marten et al. 2002; Gurwell 2004) that do not resolve Titan's disk and are thus more heavily weighted towards mid-latitudes (30°S–30°N). At latitudes northward of 45°N, the profiles are more uniform below 250–300 km while concentration minima are observed around 350–400 km for HCN and 320 km for HC_3N. The HCN minimum is more pronounced (and slightly higher)

at 50–60°N than at 80°N, leading to an HCN-depleted zone limited in latitude and altitude, as shown in Fig. 10.10 (Teanby et al. 2008b). A CIRS limb sequence at 82°N with high vertical resolution (10 km) has revealed a layered structure in the profiles of HCN and HC_3N, with variations of about an order of magnitude over a few tens of km (Teanby et al. 2007). This structure is reminiscent of the discrete haze layers seen in Cassini images (Porco et al. 2005) and might imply a close connection between hazes and nitriles.

Acetonitrile (CH_3CN) has only been observed from the ground (Marten et al. 2002). Its disk-averaged mole fraction is about 20–50 times lower than that of HCN in the 200–500 km range, slightly increasing with height from (0.8 to 4) × 10^{-8} in this interval. Below 150 km, it decreases sharply down to the condensation level around 80 km with a vertical gradient even steeper than for HC_3N.

The enrichment of hydrocarbons and nitriles in the stratosphere at winter latitudes seems to be roughly correlated with their vertical concentration gradient at low latitudes and anti-correlated with their lifetime in the stratosphere (e.g. Teanby et al. 2009; Bézard 2009). This is consistent with subsidence in the winter polar vortex, bringing air rich in photochemical compounds from their formation region in the upper atmosphere down to the stratosphere (see Sections 10.6 and 10.7 and Chapter 13). The polar vortex acts to isolate high winter latitudes but details of the hydrocarbon and nitrile distributions, such as the concentration minima observed at 350–400 km, provide evidence for dynamics more complex than predicted by general circulation models (Teanby et al. 2008b).

Above the region probed by thermal emission measurements, information is scarce. The Voyager UVS occultation data saw evidence for absorption by HCN and/or HC_3N but could not disentangle the two. The Cassini UVIS occultation at 36°S indicates a HCN mole fraction around 3 × 10^{-5} at 615 km increasing to 1 × 10^{-3} at ~1000 km (assuming a CH_4 mole fraction of 0.014) but these data may need to be reanalyzed (see Section 10.3.3). Cassini INMS detected in situ HCN, HC_3N and C_2N_2 around 1200 km at ~39°N with a mole fraction less than 5 ppm (Waite et al. 2005). Ion measurements conducted during a low-altitude pass at 1027 km near 74°N latitude were analyzed to determine indirectly the abundances of several N-bearing molecules (Vuitton et al. 2006, 2007). The HCN, HC_3N and CH_3CN mole fractions derived from INMS data are much larger than the CIRS or ground-based measurements at 500 km (about 10, 30 and 200 times respectively), which implies production in the upper atmosphere and transport or diffusion to lower levels. INMS data also provide the first evidence for the presence of cyanobutadiyne (HC_5N) at the ppm level, acrylonitrile (C_2H_3CN), propionitrile (C_2H_5CN), ammonia (NH_3), methyleneimine/methanimine (H_2CNH), probably methylcyanopolyynes (CH_3C_3N, CH_3C_5N) and two unidentified N-bearing species (C_5H_5N, C_6H_7N), which reveals the complexity of the chemistry taking place in the upper atmosphere (cf. Ch. 12).

10.5.4 Minor Constituents – Oxygen Compounds

Although Titan's atmosphere is a reducing environment, it contains oxygen compounds, three of which have been detected so far. Carbon dioxide, the first to be discovered (by *Voyager* 1 in 1980; Samuelson et al. 1983), is also the best characterized, as observations by *Voyager* 1, *Voyager* 2, *ISO*, and *Cassini* all give consistent results (see de Kok et al. 2007; Coustenis et al. 2007, and references therein). To within error bars, CO_2 appears to be uniformly mixed with latitude and altitude above its condensation level in the lower stratosphere and up to at least 200 km, with a (1.5 ± 0.4) × 10^{-8} mixing ratio. CO_2 can be easily formed through reaction of CO and OH, itself produced from the photolysis of water. CO was first discovered from ground-based observations at 1.6 μm (Lutz et al. 1983), and extensively re-observed since then, especially at 5-μm (in reflectance spectroscopy, thermal emission, and non-thermal emission) and through its mm/submm rotational lines observed from the ground and recently from *Cassini* (see Hörst et al. 2008 for a review of all measurements). Although the early observations generated a large body of controversy as to the abundance and stratospheric vertical distribution of CO, the most recent measurements point to a mean, latitude-independent, mixing ratio of about 40 ppm, with no clear evidence for altitude variation from the surface to the upper atmosphere. For both CO_2 and CO, the spatial and vertical uniformity can be understood in terms of their long chemical lifetimes (typically a few thousand and 500 million years, respectively) with respect to the horizontal and vertical transport timescales. The third oxygen species, water vapor, has been detected by ISO (Coustenis et al. 1998). The H_2O column density is $2.6^{+1.9}_{-1.6}$ × 10^{14} mol cm^{-2}, and the best-determined mixing ratio is 8^{+6}_{-4} × 10–^{9} at 400 km, although it most likely increases with altitude. A preliminary assessment of the CIRS/*Cassini* spectra indicates that water is detected in these data (Bjoraker et al. 2008), but no estimates on the amount and distribution of water are available yet. Finally, upper limits on CH_3OH and CH_3C_2O are available from INMS/*Cassini* (Vuitton et al. 2007).

The presence of H_2O and CO_2 is a direct proof of an external source of water in Titan's atmosphere, and photochemical models designed to reproduce the observed abundance of all three oxygen species require reassuringly similar OH (H_2O) fluxes (Table 10.1). The essential unsolved question is the ultimate origin of this water influx, which possibly includes distant (micrometeorite ablation) and/or

Table 10.1 Water (OH), CO, and O^+ fluxes in several chemical models. Fluxes, φ, (10^6 cm^{-2} s^{-1}) are referred to the surface

Reference	Target-molecule(s)	φ (OH)	φ (CO)	φ ($O(^3P)$)
Lara et al. (1996); Lara (1998)	CO_2, CO	3	0.83	–
Coustenis et al. 1998[a]	H_2O	1.3–4.5	–	–
Wilson and Atreya 2004	CO_2, H_2O	5	($5x10^{-5}$)[b]	–
Hörst et al. 2008[c]	CO_2, CO, H_2O	2–9	–	1–4

[a] From rescaling of Lara et al. (1996) model.
[b] Imposed mixing ratio.
[c] Including sensitivity to eddy diffusion profile.

local (sputtering of icy satellite or ring surfaces, Enceladus venting) sources.

The origin of CO is more uncertain. Early models (Samuelson et al. 1983; Yung et al., 1984; Toublanc et al. 1995; Lara et al. 1996) assumed that the formation of CO proceeds through $OH + CH_3 \rightarrow CO + 2\ H_2$ (i.e. that a flux of water *alone* could explain all three O-bearing compounds). However, even under this assumption, the OH fluxes required to sustain the observed amounts of H_2O and CO_2 fail to produce a ~ 40 ppm CO mixing ratio and the current chemical loss of CO exceeds its steady-state production by typically (1–2) × 10^6 cm^{-2} s^{-1}. The problem was exacerbated with the realization (Wong et al. 2002) that the $OH + CH_3$ reaction essentially recycles water, leading to only ~2 ppm of CO in equilibrium. Suggestions to solve this dilemma included: (i) alternate external sources, such as CO contained in micrometeorites (Lara et al. 1996) or delivered by cometary impacts (Lellouch et al. 2003), (ii) surface or internal sources such as oceanic evaporation (Dubouloz et al. 1989) or volcanic outgassing (Baines et al. 2006), and (iii) a CO abundance not in equilibrium and reflecting a larger primordial abundance (Wong et al. 2002; Wilson and Atreya 2004).

The recent discovery of O^+ ions precipitating into Titan's atmosphere (Hartle et al. 2006) provides a new source of oxygen and especially CO because through collisions with the atmosphere O^+ is ultimately converted into ground-state $O(^3P)$, which can react with CH_3 to produce CO, either directly ($O(^3P) + CH_3 \rightarrow CO + H_2 + H$) or through HCHO (Hörst et al. 2008). These authors showed that essentially all of the incoming O^+ is converted to CO, so that the observed O^+ influx rate of ~10^6 cm^{-2} s^{-1} can provide the observed CO abundance in ~300 million years and approximately balance the chemical loss of CO to CO_2. Studying the sensitivity of their model calculations to eddy diffusion profiles, Hörst et al. (2008) demonstrated that the abundances and profiles of CO, H_2O, and CO_2 can be fit simultaneously with realistic fluxes of OH (H_2O) and $O(^3P)$ (O^+) .

In Tables 10.2 and 10.3, a brief summary of Titan's stratospheric composition is given at two latitudes (15°S, 54°N) for the 5 mbar pressure level, where the altitude is 115–120 km. It should be kept in mind that the stratospheric composition varies considerably with altitude and latitude with few exceptions such as CH_4 and CO. The reader is strongly encouraged to consult Figs. 10.8–10.10 in conjunction with Tables 10.2 and 10.3.

Table 10.3 Stratospheric composition 54°N: mixing ratios (by volume) at approximately 115 km/5 mbar

Hydrocarbonspe		Nitriles		Oxygen compounds	
CH_4		HCN	0.9 ppm (1)	CO	
C_2H_6	16 ppm (1)	CH_3CN		CO_2	25 ppb (1)
C_2H_2	4 ppm[a] (1)	HC_3N	15 ppb[a] (1)	H_2O	
C_2H_4	0.6 ppm (1)	C_2N_2	1 ppb (3)		
C_3H_8	1.5 ppm (1)				
CH_3C_2H	20 ppb (1)				
C_4H_2	20 ppb[a] (1)				
C_6H_6	4 ppb[a] (1)				
H_2	0.0012 (2)				

[a] At 170 km (1 mbar).Source: (1) Vinatier (2007); (2) Courtin et al. (2008); (3) Teanby et al. (2009)

Table 10.2 Stratospheric composition 15°S: mixing ratios (by volume) at approximately 120 km/5 mbar.

Hydrocarbonspe		Nitriles		Oxygen compounds	
CH_4	0.014 (1)	HCN	0.1 ppm (2)	CO	47 ppm (7)
C_2H_6	10 ppm (2)	CH_3CN	20 ppb[a] (5)	CO_2	16 ppb (7)
C_2H_2	2 ppm (2)	HC_3N	1 ppb[a] (5)	H_2O	0.4 ppb (3)
C_2H_4	0.4 ppm (2)	C_2N_2	0.06 ppb (6)		
C_3H_8	0.5 ppm (2)				
CH_3C_2H	8 ppb (2)				
C_4H_2	1 ppb (2)			Noble	gases
C_6H_6	0.4 ppb (3)			^{36}Ar	0.28 ppm (1)
H_2	0.00096 (4)			^{40}Ar	43 ppm (1)

[a] At 300 km (disc-averaged).
Source: After Bézard 2009 with additional data points from Teanby et al. 2009; (1) Niemann et al. (2005); (2) Vinatier et al. (2007a); (3) Coustenis et al. (2007); (4) Courtin et al. (2008); (5) Marten et al. (2002); (6) Teanby et al. (2009); (7) de Kok et al. (2007)

10.5.5 Isotope Ratios

Numerous isotopic ratios have now been determined in Titan's atmosphere, either from in situ measurements (Huygens GCMS, Cassini INMS) or from spectroscopic observations at IR and mm wavelengths obtained from the ground and especially from Cassini/CIRS (see Table 10.4). Most isotopic ratios have been determined separately in several molecules, allowing one to study (i) formation and evolution processes of the atmosphere as a whole, as traced by major species and (ii) chemical fractionation effects in minor species. The interpretation of isotopic ratios in CH_4, N_2, and CO is discussed in detail in the Chapters 3 and 7. Briefly, the enhanced D/H in Titan's methane compared to the protosolar value – typically by a factor of 6 – is thought to reflect a combination of (i) an initially high D/H in the primordial icy material that formed Titan and (ii) fractionation processes at work in the atmosphere, such as methane photolysis and escape (Pinto et al. 1986; Lunine et al. 1999; Mousis et al. 2002; Cordier et al. 2008). As regards N_2, the factor ~1.5 enhancement in $^{15}N/^{14}N$ has been interpreted as due to non-thermal escape of N_2 (Lunine et al. 1999), and suggests that Titan's primitive atmosphere was 2–10 times thicker than nowadays (Niemann et al. 2005). A similar explanation, involving a massive loss of CO in Titan's early history, was put forward by Wong et al. (2002) to explain the factor of ~2 higher than terrestrial $^{18}O/^{16}O$ ratio reported by Owen et al. (1999). There is recent evidence, however, that the enrichment in ^{18}O is considerably milder (see Table 10.4). Finally, atmospheric escape is also qualitatively consistent with the fact that the $^{12}C/^{13}C$ ratio, as measured in CH_4, is slightly (by 8 %), but unambiguously, smaller than the terrestrial value of 89.

The $^{12}C/^{13}C$ ratio has been measured in many molecules besides CH_4, including CH_3D, C_2H_2, C_2H_6, HCN, HC_3N, CO,

Table 10.4 Isotopic ratios determined from indicated parent molecules and techniques for Titan's atmosphere compared with values for the Earth and the Sun

Isotope	Molecule	Technique	Titan value	Reference	Earth	Solar[e]
D/H	H_2	GCMS	$(2.3\pm0.5) \times 10^{-4}$	Niemann et al. 2005	1.56×10^{-4}	1.9×10^{-5}
	CH_4	IR, ground	$(1.25\pm0.25) \times 10^{-4}$	Penteado et al. 2005		
	CH_4	CIRS	$(1.17^{+0.23}_{-0.28}) \times 10^{-4}$	Coustenis et al. 2007		
	CH_4	CIRS	$(1.32^{+0.15}_{-0.11}) \times 10^{-4}$	Bézard et al. 2007		
	C_2H_2	CIRS	$(2.09\pm0.45) \times 10^{-4}$ [a]	Coustenis et al. 2008		
$^{12}C/^{13}C$	CH_4	GCMS	82.3±1	Niemann et al. 2005	89	89
	CH_4	INMS	~81 [b]	Waite et al. 2005		
	CH_4	CIRS	76.6±2.7	Nixon et al. 2008a		
	CH_3D	CIRS	82^{+27}_{-18}	Bézard et al. 2007		
	C_2H_2	CIRS	84.8±3.2	Nixon et al. 2008a		
	C_2H_6	CIRS	89.8±7.3	Nixon et al. 2008a		
	$CH_4+C_2H_2+C_2H_6$ [c]	CIRS	80.8±2.0	Nixon et al. 2008a		
	HCN	mm, ground	108±20 [d]	Gurwell 2004		
	HCN	CIRS	75±12	Vinatier et al. 2007b		
	HC_3N	CIRS	79±17	Jennings et al. 2008		
	CO_2	CIRS	84±17	Nixon et al. 2008b		
$^{14}N/^{15}N$	N_2	GCMS	183±5	Niemann et al. 2005	272	440±60 [f]
	N_2	INMS	168–211 [b]	Waite et al. 2005		
	HCN	mm, ground	60–70	Marten et al. 2002		
	HCN	mm, ground	72±9 [d]	Gurwell 2004		
	HCN	CIRS	56±8	Vinatier et al. 2007b		
$^{16}O/^{18}O$	CO	mm, ground	~250	Owen et al., 1999	499	499
	CO_2	CIRS	346±110	Nixon et al. 2008b		
$^{36}Ar/^{40}Ar$	atoms	GCMS	$(6.5\pm0.8) \times 10^{-3}$	Niemann et al. 2005	0.0034	3440

[a] From nadir observations. A slightly lower value $(1.63 \pm 0.27) \times 10^{-4}$ is obtained from limb observations.
[b] Estimated in lower atmosphere from extrapolation of values measured in thermosphere (95.6 ± 0.1 for $^{12}C/^{13}C$ and 172–215 for $^{14}N/^{15}N$).
[c] Weighted-mean average.
[d] Assuming thermal profile from Lellouch (1990). Higher values (132 ± 25 for $^{12}C/^{13}C$ and 94 ± 13 for $^{14}N/^{15}N$) are found when the profile from Coustenis and Bézard (1995) is used.
[e] Lodders (2003).
[f] Proto-solar value, based on the Jupiter value (Owen et al. 2001).

and CO_2. To within error bars, all measurements are consistent with the value in CH_4, although for hydrocarbons Nixon et al. (2008a) report a possible trend for an increasing value with molecular mass. In contrast, the D/H ratio measured in H_2 (Niemann et al. 2005) is somewhat higher than in CH_4, which might result from fractionation at atmospheric escape. Fractionation by photolysis may also occur. Given the higher binding energy of the C-D bond compared to C-H, this would tend to enhance the D/H ratio in C_2H_2, as marginally observed (Coustenis et al. 2008), but decrease it in H_2 . Evidence for such an effect is best seen in HCN, in which $^{15}N/^{14}N$ is about three times higher than in N_2. As demonstrated by Liang et al. (2007a), this results from the self-shielding of $^{14}N^{14}N$ against photolysis, while $^{14}N^{15}N$, whose predissociation states are shifted from those of $^{14}N^{14}N$, remains optically thin to greater depths. For pure N_2 photolysis, this would in fact lead to a $HC^{14}N/HC^{15}N$ ratio as low as 23, considerably overpredicting the observed value of ~60. This implies an additional source of non-fractionated atomic N, attributed to ion/electron impact on N_2.

10.6 Sources, Sinks, and Photochemistry of Atmospheric Composition

The atmosphere of Titan contains many trace constituents in the form of hydrocarbons (C_xH_y), nitriles ($C_xH_yN_z$) and aerosols, which are products of the photolysis of methane and nitrogen in the upper atmosphere. Even before Voyager discovered this suite of constituents and that the atmosphere was primarily nitrogen, Strobel (1974) developed the basic framework of methane photochemistry in Titan's atmosphere and concluded that, in the absence of escaping hydrogen atoms and molecules being recaptured, methane would be irreversibly destroyed on a time scale short compared to Titan's age. Yung et al. (1984) developed the first comprehensive post-Voyager model of Titan photochemistry that explained satisfactorily the limited composition data from Voyager.

The photochemistry of CH_4 occurs in two distinct, broad altitude/pressure regions. When coupled with the high efficiency for hydrogen escape, it leads to irreversible loss of CH_4. In addition, CH_4 may be escaping the atmosphere at large rates (cf. Yelle et al. 2008; Strobel 2008, 2009). The lifetime for atmospheric CH_4 (for column density ~7.5×10^{24} cm^{-2}) is only ~45 MY when its loss rate is constrained by its limiting flux through the lower stratosphere and ~15 MY when it is constrained by the largest model chemical loss rate (see Table 10.5 and discussion below) and implies that it must be continually resupplied from the interior. (Table 10.5 below provides a convenient list of all loss rates and fluxes discussed in this section for easy reference.) Direct CH_4 photolysis is driven principally by the intense solar Lyman α line at 121.6 nm, because UV radiation is only absorbed by CH_4 with a significant cross section below 145 nm, even though only 4.5 eV (= 285 nm) is needed to break CH_4 apart. This photolysis is centered at pressures ~7 nbar (~825 km) and in photochemical models contributes a net destruction rate of ~2.9×10^9 cm^{-2} s^{-1} (e. g. Yung et al. 1984). The radicals released in CH_4 photolysis react to form initially C_2H_y hydrocarbons (C_2H_6, C_2H_4, C_2H_2). Methane can also be destroyed by indirect catalytic C_2H_2 dissociation, whereby the radicals C_2H and C_2 dissociate CH_4 and recycle C_2H_2. This process is most important in the 0.1–1 mbar region (190–300 km) and contributes a loss rate of ~1×10^{10} cm^{-2} s^{-1}, significantly larger than the direct rate. To a lesser extent, methane is also destroyed by ion chemistry, with two CH_4 molecules dissociated per ion pair created. From Wilson and Atreya (2004) their globally averaged, integrated electron production rate times 2 is ~3.6×10^8 cm^{-2} s^{-1} or when referenced to the surface ~7×10^8 CH_4 cm^{-2} s^{-1}, are destroyed.

Thus an upward flux of CH_4 driven by photochemistry, must be balanced by downward fluxes of more complex, C_2, C_3, C_4, etc., hydrocarbons carrying the same total number of

Table 10.5 Comparison of various rates for CH_4 photochemistry, escape fluxes from, and limiting diffusion fluxes through Titan's atmosphere

Process	Rates referenced to surface (cm^{-2} s^{-1})
H_2 escape flux at exobase	Y: 7.2×10^9; WA: 5.0×10^9; L: 4.2×10^9; C:1.4×10^{10}; S9: 1.1×10^{10}
H escape flux at exobase	Y: 5.5×10^9; WA: 3.0×10^9; L: 9.3×10^8
CH_4 escape flux at exobase	Yelle08: (2.5–3) × 10^9; S9: 2.1×10^9
Ionospheric chemical CH_4 loss[(a)]	WA: ~7×10^8
Direct (Ly α) CH_4 dissociation[a]	Y: 2.9×10^9
C_2H_2 catalytic CH_4 dissociation[a]	Y: 1.1×10^{10}
Total net CH_4 chemical loss[(a)] and gas phase C atom flux	Y: 1.5×10^{10}; WA: 8.7×10^9; L: 1.3×10^{10}
Downward C_2H_6 flux at tropopause	Y: 5.8×10^9; WA: 2.2×10^9; L: 4.1×10^9
Downward C_2H_2 flux at tropopause	Y: 1.2×10^9; WA: 5.9×10^8; L: 3.2×10^8
Downward C_3H_8 flux at tropopause	Y: 1.4×10^8; WA: 2.9×10^8; L: 3.7×10^8
Downward mass flux of aerosols	L: 1.5×10^{-14}; B: 1.5×10^{-14}; M: (0.5–2) × 10^{-14} g cm^{-2} s^{-1}
Downward C atom flux in aerosols	L: 3.8×10^8
Downward N atom flux in aerosols	L: 3.0×10^8
Downward H atom flux in aerosols	L: 2.9×10^8
Limiting flux of H_2 (@0.4%)	S08: 1.3×10^{10}

Y: Yung et al. (1984); WA: Wilson and Atreya (2004); C: Cui et al. (2008); L: Lavvas et al. (2008); S8: Strobel (2008); S9: Strobel (2009); Yelle08: Yelle et al. (2008); B: Bézard (2009); M: McKay et al. (2001).

[a] Rate = $\int_{r_0}^{r_{ex}} L(r)(r^2 / r_0^2)dr$, r_0, r_{ex} = Titan's radius, exobase.

carbon atoms. All of these less saturated hydrocarbons condense as liquids or solids in the lower stratosphere and vicinity of Titan's cold tropopause (~70 K), with the exception of C_2H_4, to form a pervasive haze layer. Eventually they precipitate from the atmosphere and accumulate on the surface, although to date the precise composition, location, and depth of these end products of CH_4 photolysis is still under intense study by Cassini scientists (cf. Chapter 6). The most abundant photolysis product is C_2H_6 (cf. Figs. 10.8–10.10), which is expected to undergo condensation in the stratosphere 40–50 km above the surface.

The tentative detection of benzene (C_6H_6) at ppbv levels by ISO (Coustenis et al. 2003), added a new dimension to Titan photochemistry, as benzene is the first ring molecule that is generally a precursor to a whole host of heavier hydrocarbons including polycyclic aromatic hydrocarbons (PAH's). Aerosols can form upon polymerization of the PAH's. The only aerosols predicted prior to the detection of benzene were from polyyne ($C_{2n}H_2$) polymers, HCN polymers, and the condensation of stable C_2–C_4 hydrocarbons in the lower stratosphere. Wilson and Atreya (2004) developed a comprehensive post-ISO model of the coupled chemistry of the neutral atmosphere and the ionosphere. A simplified chemical scheme for the neutral atmosphere from Atreya et al. 2006 is shown in Fig. 10.11. Waite et al. (2007) reported molecules as large as tens of thousand daltons may be present at ionospheric heights, which are probably precursors to aerosol formation in the thermosphere. Cassini UVIS has detected aerosols from 1000 km down to the main haze layer (Liang et al. 2007b).

Synthesis of complex hydrocarbons can be defeated by H-atom cracking reactions: e. g., $H + C_{2n}H_2 + M \rightarrow C_{2n}H_3 + M$, $H + C_{2n}H_3 \rightarrow C_2H_2 + C_{2n-2}H_2$. Since the main Titan haze layer is composed of large, condensed molecules with most of the mass contributed by hydrocarbons, Titan must somehow limit the efficiency of these H-atom cracking reactions. The haze particles may play a fundamental role in this process by suppressing the H atom concentration via heterogeneous reactions which recombine H atoms on aerosol surfaces and release H_2 gas (cf. Lebonnois et al. 2003a; Sekine et al. 2008a, b). These heterogeneous reactions are more than competitive with the cracking reactions that are slow at Titan's pressures and temperatures.

The key observational facts constraining CH_4 photochemistry are (1) the INMS inferred H_2 escape rate of (1.1–1.4) × 10^{10} cm^{-2} s^{-1} (Cui et al. 2008; Strobel 2009), (2) the most abundant photochemically produced gas phase hydrocarbon molecule is C_2H_6 followed by C_2H_2 (cf. Figs. 10.8, 10.10), (3) the stratospheric CH_4 mole fraction is 0.0141 from GCMS (Niemann et al. 2005), and (4) the thermospheric CH_4 mole fraction obtained by INMS at the lowest altitudes sampled is slightly lower than the stratospheric value (Yelle et al. 2008) and indicative of CH_4 destruction. Bézard (2009) inferred the mass production rates of C_2H_6 and haze from CIRS derived C_2H_6 and DISR derived haze profiles under the assumption that diffusive transport dominates below their respective formation regions. He obtained a production ratio of 15 times more C_2H_6 than haze.

From a large number of photochemical model calculations, three were selected to illustrate mass balance and partitioning of photochemical products: (1) Yung et al. (1984) for comprehensive post-Voyager analysis, (2) Wilson and Atreya (2004), and (3) Lavvas et al. (2008) for contemporary Cassini–Huygens analysis. Table 10.5 gives relevant magnitudes of CH_4 destruction rates, and downward, escape, and limiting fluxes that pertain to CH_4 photochemistry. In spite of the 24 year time span and improvement in input quantities and more observational constraints, Yung et al. (1984) and Lavvas et al. (2008) are in essential agreement on these important rates. In addition to these gas phase production rates, Lavvas et al. (2008) calculated individual production rates of C, N, H atoms that are incorporated into haze particles

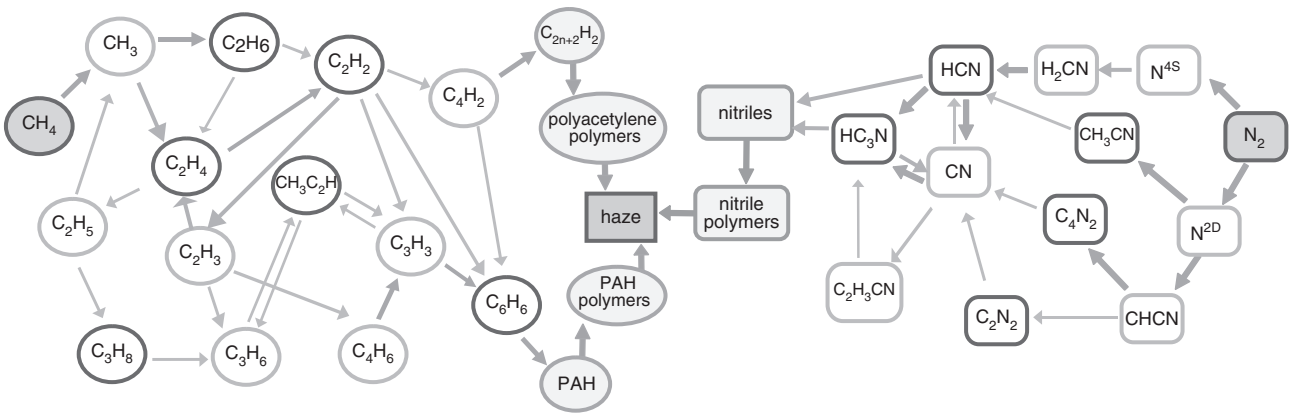

Fig. 10.11 Simplified schematic of the photochemistry of N_2 and CH_4 in Titan's atmosphere through the formation of polymers (after Atreya et al. (2006))

and the total haze production rate (cf. Table 10.5). This latter value is 1/14 of the gas phase mass production rate of C_2H_6, as Bézard (2009) concluded from an empirical analysis of Cassini and Huygens data. But Atreya et al. (2006) argued that this ratio may be as large as ½, based on Wilson and Atreya (2004) whose gas phase production rates are systematically lower than Yung et al. (1984) and Lavvas et al. (2008).

The chemical loss and escape of CH_4 must be balanced by upward transport from the lower atmosphere. With the further hypothesis that CH_4 is the source of all other carbon and hydrogen bearing molecules in the atmosphere and escaping from the atmosphere, then stoichiometrically 2 $CH_4 \rightarrow C_2H_{2n}$ + (4-n) H_2 must hold. Note for n = 0, the measured INMS H_2 escape rate places a lower limit on the net CH_4 destruction rate of (5.5–7) × 10^9 cm^{-2} s^{-1}. From Table 10.5 a comparison of the INMS inferred H_2 escape rates with total net CH_4 model loss rates suggests that n = 2 would be the preferred value. But observations indicate that C_2H_6 is the dominant product which implies n = 3. From the Yung et al. (1984) the effective H_2 (H_2 + ½ H) escape rate is ~1 × 10^{10} cm^{-2} s^{-1}, the lower end of INMS H_2 values, whereas Wilson and Atreya (2004) and Lavvas et al. (2008), calculated less, 0.65 × 10^{10} and 0.47 × 10^{10} cm^{-2} s^{-1}, respectively. But certainly some hydrogen is escaping in atomic form, as ionospheric chemistry leads to production of H atoms high in the atmosphere. Thus models to date under predict the H_2 escape rate, because prior to the INMS measurements it was thought that H_2 escape occurred at the Jeans rate, a factor of ~3 lower. To achieve the larger INMS H_2 escape rate and still have C_2H_6 the dominant product of CH_4 chemistry, the CH_4 chemical destruction rate must be also larger than the values given in Table 10.5.

The photochemistry of N_2 occurs mostly in Titan's thermosphere and ionosphere, because the N_2 bond strength of 9.7 eV requires energetic photons, electrons, and ion to break the molecule apart. With no optically allowed excitation paths into repulsive electronic states, dissociation occurs preferentially by indirect paths. Solar radiation between 80 and 100 nm can excite predissociating electronic states which are ≤ 25 % of the total source of N atoms (Liang et al. 2007a). The ion chemistry of N_2^+ preserves the N_2 bond, but dissociative ionization of N_2 by either electron impact or solar EUV radiation will produce one N atom and one N^+ ion, which will react with CH_4 to yield either an N atom or an ion (H_2CN^+ or HCN^+). The latter ion reacts with CH_4 to form the former ion and recombination of H_2CN^+ produces the nitrile HCN and net loss of CH_4. Energetic electrons of photolytic and magnetospheric origins can also directly dissociate N_2. The net efficiency for producing nitriles depends on the extent of self destruction of odd nitrogen by the reaction N + NH → N_2 + H. Photochemical models estimate the net production/downward flux of N atoms from the thermosphere ~(0.5–1) × 10^9 cm^{-2} s^{-1}, whereas self destruction by the above reaction limits the downward HCN flux to only ~3 × 10^8 cm^{-2} s^{-1} and an equal number incorporated into haze particles (Lavvas et al. 2008). Once the CN bond is formed, it is preserved down through the stratosphere.

10.7 Chemistry and Transport of Atmospheric Constituents

Both Voyager IRIS and Cassini CIRS spectra imply that there is enrichment of several organic compounds at high northern latitude during northern winter and early northern spring. Because most of these species are formed high up in the atmosphere from the photo- and electron-impact dissociation of CH_4 and N_2, their mixing ratio surfaces increase with altitude. A meridional circulation tilts these mixing ratio surfaces in the following sense (cf. Holton and Schoeberl 1988; Bacmeister et al. 1995; Dire 2000). Downward motion (subsidence) brings down higher mixing ratios from above while upward motion brings lower mixing ratios from below. Hence enrichment with latitude implies subsidence over Titan's North Pole in its current winter season during the Cassini Nominal Mission. In Fig. 10.12 is a schematic diagram of what is thought to be the relevant dynamical processes that generate constituent transport and based on analogy with the much better understanding of these processes in the Earth's middle atmosphere. In Fig. 10.10 there are blue dashed lines that show the region where horizontal potential vorticity gradients are the steepest (~55–65° N) and location of dynamical mixing barriers. In this figure the more abundant C_2H_2 and HCN clearly show enhanced mixing ratios in the northern polar region at high altitudes expected from subsidence. In the case of HCN, most of its formation occurs at higher altitudes, whereas for C_2H_2 there is also significant formation in the stratosphere. However, C_2H_2 has a local maximum in mixing ratio at ~200 km in the polar night suggesting a local source and certainly not consistent with simple explanation from subsidence associated with a meridional circulation. On the other hand HCN has a local minimum in its mixing ratio center at ~350 km and 60° N. This cannot be due to gas phase conversion to other gas phase nitriles, e. g. H_3CN in Fig 10.10. But it could be due to heterogeneous reactions removing nitriles and/or condensation, although the temperature is still warm by Titan's standards. Chapter 13 discusses dynamics in much more detail.

10.8 Concluding Remarks

At the end of the Cassini–Huygens Nominal Mission, we have a good first order knowledge of the composition and thermal structure of the atmosphere with the exception of the

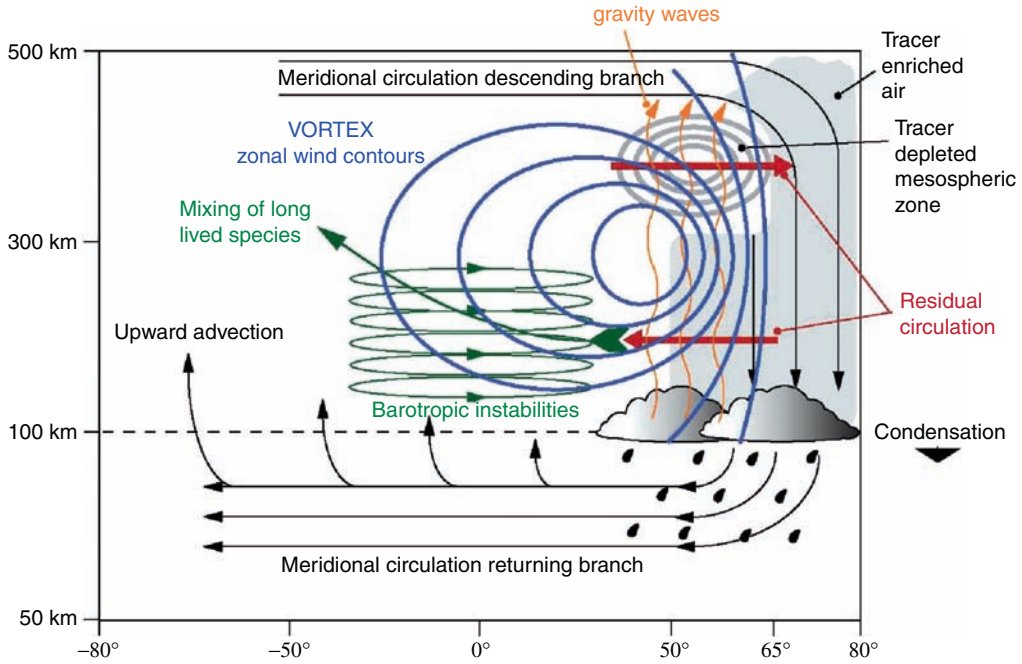

Fig. 10.12 Schematic of dynamical processes thought to be important in Titan's winter north polar region: a single cell meridional circulation, a polar vortex of strong zonal winds, wave induced mixing by inferred equatorial barotropic and gravity waves (after Teanby et al. (2008))

~500–950 km region, variously called the ignorosphere, agnostosphere, etc. Although HASI inferred the thermal structure at equatorial latitudes through this region, it did not yield a pronounced mesopause widely expected from theory. Ground-based millimeter-wavelength provided limited, globally averaged, composition measurements, in comparison to the detailed altitudinal and latitudinal composition and temperature measurements by CIRS for the stratosphere. The UVIS stellar occultation could also provide composition and thermal structure in the ignorosphere region, but the only published analysis (Shemansky et al. 2005) has deficiencies noted above. Better knowledge of the ignorosphere structure would be helpful to resolve the vexing factor of ~2.5 density discrepancy among HASI, INMS, and AACS.

The thermosphere is a chemical factory that initiates the formation of complex positive and negative ions in the high thermosphere as a consequence of magnetospheric–ionospheric–atmospheric interaction involving solar EUV and UV radiation, energetic ions and electrons. This factory produces very heavy positive and negative ions and large molecules, e.g., benzene, naphthalene, nitriles, which apparently condense out and are detectable in solar and stellar UV occultations at ~1000 km (Liang et al. 2007a), and initiate the haze formation process. As these particles fall through the ignorosphere and grow, they become detectable by remote sensing: UVIS at ~1000 km, ISS at ~500 km and eventual become ubiquitous throughout the stratosphere. These haze particles are strong absorbers of solar UV and visible radiation and play a fundamental role in heating Titan's stratosphere and perhaps the ignorosphere (Lavvas et al. 2009). The differential heating with latitude drives wind systems in Titan's middle atmosphere, much as ozone does in the Earth's middle atmosphere. How intimately coupled is the upper thermosphere with the stratosphere and what is the role of the ignorosphere? It is certainly the region of direct photolysis of CH_4. Are complex positive and negative ions and large molecules from above necessary for formation of the main haze layer? What is the role of heterogeneous reactions in determining the partitioning of gas phase molecules and the composition of haze particles?

The Cassini Mission has just entered the first extended mission known as the Cassini Equinox Mission to understand the transition for solstitial conditions to equinoctial conditions, especially as the northern polar region emerges out of the polar night and the polar vortex breaks up. In the planning stages is a proposal to extend the Cassini Mission into a northern, summer solstice mission to explore that transition from equinox into solstitial conditions. Thus the entire duration of the Cassini Mission would be a half of Saturnian year and would permit observations of a full seasonal cycle on Titan.

Acknowledgments DFS acknowledges support by the Cassini–Huygens Mission through JPL Contract No. 1280253. SKA acknowledges support by the Cassini–Huygens Program and Planetary Atmospheres Program of NASA. BB, EL, and M Fulchignoni acknowledge financial support from CNRS and CNES. The authors are indebted to Dr. Sandrine Vinatier for providing Fig. 10.9 and Dr. Eric Wilson supplying his rates referenced to the surface in Table 10.5.

References

Achterberg RK, Conrath BJ, Gierasch PJ, Flasar FM, Nixon CA (2008) Titan's middle-atmospheric temperatures and dynamics observed by the Cassini Composite Infrared Spectrometer. Icarus 194:263–277, doi:10.1016/j.icarus.2007.09

Atreya SK, Donahue TM, Kuhn WR (1978) Evolution of a nitrogen atmosphere on Titan. Science 201:611–613

Atreya SK, Adams EY, Niemann HB, Demick-Montelara JE, Owen TC, Fulchignoni M, Ferri F, Wilson EH (2006) Titan's methane cycle. Planet Space Sci 54:1177–1187. doi:10.1016/j.pss.2006.05.028

Bacmeister JT, Schoeberl MR, Summers ME, Rosenfield JR, Zhu X (1995) Descent of long-lived trace gases in the winter polar vortex. J Geophys Res 100:11669–11684

Baines KH, Drossart P, Lopez-Valverde MA, Atreya SK, Sotin C, Momary TW, Brown RH, Buratti BJ, Clark RN, Nicholson PD (2006) On the discovery of CO nighttime emissions on Titan by Cassini/VIMS: derived stratospheric abundances and geological implications. Planet Space Sci 54:1552–1562. doi:10.1016/j.pss.2006.06.020

Bézard B (2009) Composition and chemistry of Titan's stratosphere. Phil Trans Royal Soc A 367:683–695. doi:10.1098/rsta.2008.0186

Bézard B, Coustenis A, McKay CP (1995) Titan's atmospheric temperature asymmetry: a radiative origin? Icarus 111:267–276

Bézard B, Nixon CA, Kleiner I, Jennings DE (2007) Detection of $^{13}CH_3D$ on Titan. Icarus 191:397–400

Bjoraker G, Achterberg R, Anderson C, Samuelson R, Carlson R, Jennings D (2008) Cassini/CIRS observations of water vapor in Titan's stratosphere, Bull Amer Astron Soc 40(31.12):446

Broadfoot AL et al (1981) Extreme ultraviolet observations from Voyager 1 encounter with Saturn. Science 212:206

Cordier D, Mousis O, Lunine JI, Moudens A, Vuitton V (2008) Photochemical enrichment of deuterium in Titan's atmosphere: new insights from Cassini–Huygens. Astrophys J Lett 689:L61–L64

Courtin R, Gautier D, McKay CP (1995) Titan's thermal emission spectrum: reanalysis of the Voyager infrared measurements. Icarus 114:114–162

Courtin RD, Sim C, Kim S, GautierD, Jennings DE (2008) Latitudinal variations of tropospheric H_2 on Titan from the Cassini CIRS investigation. 40th DPS meeting Abstract. 31.01, Ithaca, New York, Bull Amer Astron Soc 40(31.01): 446

Coustenis A, Bézard B (1995) Titan's atmosphere from Voyager infrared observations. IV. Latitudinal variations of temperature and composition. Icarus 115:126–140

Coustenis A, Salama A, Lellouch E, Encrenaz T, Bjoraker GL, Samuelson RE, de Graauw T, Feuchtgruber H, Kessler MF (1998) Evidence for water vapor in Titan's atmosphere from ISO/SWS data. Astron Astrophys 336:L85–L89

Coustenis A, Salama A, Schulz B, Ott S, Lellouch E, Encrenaz TH, Gautier D, Feuchtgruber H (2003) Titan's atmosphere from ISO mid-infrared spectroscopy. Icarus 161:383–403. doi:10.1016/S0019-1035(02)00028-3

Coustenis A, Achterberg RK, Conrath BJ, Jennings DE, Marten A, Gautier D, Nixon CA, Flasar FM, Teanby NA, Bézard B, Samuelson RE, Carlson RC, Lellouch E, Bjoraker GL, Romani PN, Taylor FW, Irwin PGJ, Fouchet T, Hubert A, Orton GS, Kunde VG, Vinatier S, Mondellini J, Abbas MM, Courtin R (2007) The composition of Titan's stratosphere from Cassini/CIRS mid-infrared spectra. Icarus 189:35–62. doi:10.1016/j.icarus.2006.12.022

Coustenis A, Jennings DE, Jolly A, Bénilan Y, Nixon CA, Vinatier S, Gautier D, Bjoraker G, Romani P, Carlson R, Flasar FM (2008) Detection of C_2HD and the D/H ratio on Titan. Icarus 197:539–548. doi:10.1016/j.icarus.2008.06.003

Crespin A, Lebonnois S, Vinatier S, Bézard B, Coustenis A, Teanby NA (2008) Diagnostics of Titan's stratospheric dynamics using Cassini/CIRS data and the 2-dimensional IPSL Circulation Model. Icarus 197:556–57. doi:10.1016/j.icarus.2008.05.010

Cui J, Yelle RV, Volk K (2008) Distribution and escape of molecular hydrogen in Titan's thermosphere and exosphere. J Geophys Res 113:E10004. doi:10.1029/2007JE003032

Danielson RE, Caldwell J, Larach DR (1973) An inversion in the atmosphere of Titan. Icarus 20:437–443

de Kok R, Irwin PGJ, Teanby NA, Lellouch E, Bezard B, Vinatier S, Nixon CA, Fletcher L, Howett C, Calcutt SB, Bowles NE, Flasar FM, Taylor FW (2007) Oxygen compounds in Titan's stratosphere as observed by Cassini CIRS. Icarus 186:354–363. doi:10.1016/j.icarus.2006.09.016

Dire JR (2000) Seasonal photochemical and meridional transport model for the stratosphere of Titan, Icarus, 145:428–444 (cf. Bull.A. A. S., 24:955–956, 1992)

Dubouloz N, Raulin F, Lellouch E, Gautier D (1989) Titan's hypothesized ocean properties – The influence of surface temperature and atmospheric composition uncertainties. Icarus 82:81–96. doi:10.1016/0019-1035(89)90025-0

Flasar FM et al (2005) Titan's atmospheric temperatures, winds, and composition. Science 308:975–978

Fulchignoni M, Ferri F, Angrilliet F et al (2005) Titan's physical characteristics measured by the Huygens Atmospheric Structure Instrument (HASI). Nature 438:785–791. doi:10.1038/nature04314

Gillett FC, Forrest WJ, Merrill KM (1973) 8–13 micron observations of Titan. Astrophys J 187:L37–L38

Gurwell MA (2004) Submillimeter observations of Titan: Global measures of stratospheric temperature, CO, HCN, HC3N, and the isotopic 12C/13C and 14N/15N. Astrophys J 616:L7–L10

Hanel RA et al (1981) Infrared observations of the Saturnian system from Voyager 1. Science 212:192–200

Hartle RE, Sittler EC, Neubauer FM, Johnson RE, Smith HT, Crary F, McComas DJ, Young DT, Coates AJ, Simpson D, Bolton S, Reisenfeld D, Szego K, Berthelier JJ, Rymer A, Vilppola J, Steinberg JT, Andre N (2006) Preliminary interpretation of Titan plasma interaction as observed by the Cassini Plasma Spectrometer: comparisons with Voyager 1. Geophys Res Lett 33:8201. doi:10.1029/2005GL024817

Holton JR, Schoeberl MR (1988) The role of gravity wave generated advection and diffusion in transport of tracers in the mesosphere. J Geophys Res 93:11075–11082

Hörst S, Vuitton V, Yelle RV (2008) The origin of oyxgen species in Titan's atmosphere. J Geophys Res 113:E10006. doi:10.1029/2008JE003135

Hunten D M (1974) The atmosphere of Titan. Washington, NASA SP-340

Hunten DM (1978) A Titan atmosphere with a surface temperature of 200 K. In Hunten DM, Morrison D (eds) The Saturn System, NASA Conf. Publ. 2068, Washington DC, pp 127–140

Hunten DM, Morrison D (eds) (1978) The Saturn System, NASA Conf. Publ. 2068, WashingtonDC, pp 127–140

Jacquemart D, Lellouch E, Bézard B, de Bergh C, Coustenis A, Lacome N, Schmitt B, Tomasko M (2008) New laboratory measurements of CH_4 in Titan's conditions and a reanalysis of the DISR near-surface spectra at the Huygens landing site. Planet Space Sci 56:613–623

Jennings DE, Nixon CA, Jolly A, Bézard B, Coustenis A, Vinatier S, Irwin PGJ, Teanby N, Romani PN, Achterberg RK, Flasar FM (2008) Isotopic ratios in Titan's atmosphere from Cassini CIRS limb sounding: HC_3N in the north. Astrophys J Lett 681:L109–L111

Jennings DE, Flasar FM, Kunde VG, Samuelson RE, Pearl JC, Nixon CA, Carlson RC (2009) Titan's surface brightness temperatures, Astrophys J, 691:L103–L105

Kuiper GP (1944) Titan: A satellite with an atmosphere. Astrophys J 100:378–383

Lara L (1998) Correction to "Vertical distribution of Titan's atmospheric neutral constituents" by L M Lara et al., J Geophys Res 103:(E11), 25775–25775

Lara LM, Lellouch E, L´opez-Moreno JJ, Rodrigo R (1996) Vertical distribution of Titan's atmospheric neutral constituents. J Geophys Res 101:23261–23283, doi:10.1029/96JE02036

Lavvas PP, Coustenis A, Vardavas IM (2008) Coupling photochemistry with haze formation in Titan's atmosphere, Part II: Results and validation with Cassini/Huygens data. Planet Space Sci 56:67–99

Lavvas PP, Yelle RV, Vuitton V (2009) The detached haze layer in Titan's mesosphere, Icarus, in press

Lebonnois S, Bakes ELO, McKay CP (2003a) Atomic and molecular hydrogen budget in Titan's atmosphere. Icarus 161:474–485. doi:10.1016/S0019-1035(02)00039-8

Lebonnois S, Hourdin F, Rannou P, Luz D, Toublanc D (2003b) Impact of the seasonal variations of composition on the temperature field of Titan's stratosphere. Icarus 163:164–174

Lellouch E (1990) Atmospheric models of Titan and Triton. Ann Geophys 8:653–660

Lellouch E, Coustenis A, Gauthier D, Raulin F, Dubouloz N, Frere C (1989) Titan's atmosphere and hypothesized ocean: a reanalysis of the Voyager 1 radio-occultation and IRIS 7.7 μm Data, Icarus, 79:328–349

Lellouch E, Coustenis A, Sebag B, Cuby J-G, L'opez-Valverde M, Schmitt B, Fouchet T, Crovisier J (2003) Titan's 5-μm window observations with the Very Large Telescope. Icarus 162:125–142. doi:10.1016/S0019-1035(02)00079-9

Lewis JS (1971) Satellites of the outer planets: Their physical and chemical nature. Icarus 15:174–185

Liang M-C, Heays AN, Lewis BR, Gibson ST, Yung YL (2007a) Source of nitrogen isotope anomaly in HCN in the atmosphere of Titan. Astrophys. J. 664:L115–L118

Liang M-C, Yung YL, Shemansky DE (2007b) Photolytically generated aerosols in the mesosphere and thermosphere of Titan. Astrophys J 661:L199–L202

Lindal GF, Wood GE, Hotz HB, Sweetnam DN (1983) The atmosphere of Titan: an analysis of the Voyager radio occultation measurements. Icarus 53:348–363

Lodders K (2003) Solar system abundances and condensation temperatures of the elements. Astrophys J 591:220–1247

Lunine JI, Yung YL, Lorenz RD (1999) On the volatile inventory of Titan from isotopic abundances in nitrogen and methane. Planet Space Sci 47:1291–1303

Lutz BL, de Bergh C, Owen T (1983) Titan–Discovery of carbon monoxide in its atmosphere. Science 220:1374–1376

Marten A, Hidayat T, Biraud Y, Moreno R (2002) New millimeter heterodyne observations of Titan: Vertical distributions of nitriles HCN, HC_3N, CH_3CN, and the isotopic ratio $^{15}N/^{14}N$ in its atmosphere. Icarus 158:532–544

McKay CP, Pollack JB, Courtin R (1989) The thermal structure of Titan's atmosphere. Icarus 80:23–53

McKay CP, Coustenis A, Samuelson RE, Lemmon MT, Lorenz RD, Cabane M, Rannou P, Drossart P (2001) Physical properties of the organic aerosols and clouds on Titan. Planet Space Sci 49:79–99

Mousis O, Gautier D, Coustenis A (2002) The D/H Ratio in methane in Titan: origin and history. Icarus 159:156–165

Müller-Wodarg ICF, Yelle RV, Cui J, Waite HJ Jr (2008) Horizontal structure and dynamics of Titan's thermosphere. J Geophys Res 113:E10005. doi:10.1029/2007JE003033

Niemann HB et al (2005) The abundances of constituents of Titan's atmosphere from the GCMS instrument on the Huygens probe. Nature 438:779–784. doi:10.1038/nature.04122

Nixon CA, Achterberg RK, Vinatier S, Bézard B, Coustenis A, Irwin PGJ, Teanby NA, de Kok R, Romani PN, Jennings DE, Bjoraker GL, Flasar FM (2008a) The 12C/13C isotopic ratio in Titan hydrocarbons from Cassini/CIRS infrared spectra. Icarus 195:778–791. doi:10.1016/j.icarus.2008.01.012

Nixon CA, Jennings DE, Bézard B, Teanby NA, Achterberg RK, Coustenis A, Vinatier S, Irwin PGJ, Romani PN, Hewagama T, Flasar FM (2008b) Isotopic ratios in Titan's atmosphere from Cassini CIRS limb sounding: CO2 in the equator and south. Astrophys J Lett 681:L101–L103

Owen T, Biver N, Marten A, Matthews H Meier R (1999) Saturn VI (Titan). IAU Circ 7306

Owen T, Mahaffy PR, Niemann HB, Atreya S, Wong M (2001) Protosolar Nitrogen. Astrophys. J. 553:L77–L79

Penteado PF, Griffith CA, Greathouse K, de Bergh C (2005) Measurements of CH3D and CH4 in Titan from infrared spectroscopy, Astrophys J 629:L53–L56

Pinto JP, Lunine JI, Kim S-J, Yung YL (1986) The D to H ratio and the origin and evolution of Titan's atmosphere. Nature 319:388–390

Porco CC et al (2005) Imaging of Titan from the Cassini spacecraft. Nature 434:159–168

Rannou P, Hourdin F, McKay CP (2002) A wind origin for Titan's haze structure. Nature 418:853–856

Roe HG, de Pater I, McKay CP (2004) Seasonal variation of Titan's stratospheric ethylene (C_2H_4) observed. Icarus 169:440–461

Samuelson RE, Maguire WC, Hanel RA, Kunde VG, Jennings DE, Yung YL, Aikin AC (1983) CO_2 on Titan. J Geophys Res 88:8709–8715

Samuelson RE, Nath NR, Borysow A (1997) Gaseous abundances and methane supersaturation in Titan's troposphere. Planet Space Sci 45:959–980

Sekine Y, Lebonnois S, Imanaka H, Matsui T, Bakes ELO, McKay CP, Khare BN, Sugita S (2008a) The role of organic haze in Titan's atmospheric chemistry: II. Effect of heterogeneous reaction to the hydrogen budget and chemical composition of the atmosphere. Icarus 194:201–211. doi:10.1016/j.icarus.2007.08.030

Sekine Y, Imanaka H, Matsui T, Khare BN, Bakes ELO, McKay CP, Sugita S (2008b) The role of organic haze in Titan's atmospheric chemistry: I. Laboratory investigation on heterogeneous reaction of atomic hydrogen with Titan tholin. Icarus 194:186–200. doi:10.1016/j.icarus.2007.08.031

Shemansky DE, Stewart AIF, West RA, Esposito LW, Hallett JT, Liu X (2005) The Cassini UVIS Stellar Probe of the Titan Atmosphere. Science 308:978–982. doi:10.1126/science.1111790

Sicardy B, Colas F, Widemann T, et al. (2006) The two stellar occultations of November 14, 2003, J Geophys Res 111, doi:10.1029/2005JE002624

Strobel DF (1974) The Photochemistry of Hydrocarbons in the atmosphere of Titan. Icarus 21:466–470

Strobel, DF (2008) Titan's hydrodynamically escaping atmosphere, Icarus, 193:588–594, doi:10.1016/j.icarus.2007.08.014

Strobel, DF (2009) Titan's hydrodynamically escaping atmosphere: escape rates and the structure of the exobase region, Icarus 202: 632–641, doi:10.1016/j.icarus.2009.03.007

Strobel DF, Shemansky DE (1982) EUV Emission from Titan's upper atmosphere: Voyager 1 encounter. J Geophys Res 87:1361

Strobel DF, Sicardy B (1997) Gravity wave and wind shear models. In: Lebreton JP (ed) HUYGENS Science, Payload and Mission, ESA SP, vol 1177, pp 299–311

Strobel DF, Hall DT, Zhu X, Summers ME (1993) Upper limit on Titan's atmospheric argon abundance. Icarus 103:333–336

Teanby NA et al (2006) Latitudinal variations of HCN, HC_3N and C_2N_2 in Titan's stratosphere derived from Cassini CIRS data. Icarus 181:243–255

Teanby NA et al (2007) Vertical profiles of HCN, HC_3N and C_2H_2 in Titan's atmosphere derived from Cassini/CIRS data. Icarus 186:364–384

Teanby NA, et al. (2008) Titan's polar vortex structure revealed by chemical tracers. J Geophys Res, 113:E12003, doi:10.1029/2008JE003218

Teanby NA et al. (2009) Titan's stratospheric C_2N_2, C_3H_4, and C_4H_2 abundance from Cassini/CIRS far-infrared spectra. Icarus, 202, 620–631, doi:10.1016/j.icarus.2009.03.022

Teanby NA, Irwin PGJ, de Kok R, Nixon CA (2009) Dynamical implications of seasonal and spatial variations in Titan's stratospheric composition. Phil Trans Royal Soc A 367:697–711, doi10.1098/rsta.2008.0164

Tomasko M, Bézard B, Doose L, Engel S, Karkoschka E, Vinatier S (2008) Heat balance in Titan's atmosphere. Planet Space Sci 56: 648–659. doi:10.1016/j.pss.2007.10.012

Toublanc D, Parisot JP, Brillet J, Gautier D, Raulin F, McKay CP (1995) Photochemical modeling of Titan's atmosphere. Icarus, 113:2–26. doi:10.1006/icar.1995.1002

Trafton LM (1972) On the possible detection of H_2 in Titan's atmosphere. Astrophys J 175:285–293

Vervack RJ Jr, Sandel BR, Strobel DF (2004) New perspectives on Titan's upper atmosphere from a reanalysis of the Voyager 1 UVS solar occultations. Icarus 170:91–112

Vinatier S (2007) Analyse des spectres infrarouges thermiques émis par l'atmosphère de Titan enregistrés par l'instrument Cassini/CIRS. Ph.D. Thesis. University of Denis Diderot, Paris VII

Vinatier S et al (2007a) Vertical abundance profiles of hydrocarbons in Titan's atmosphere at 15°S and 80°N retrieved from Cassini/CIRS spectra. Icarus 188:120–138

Vinatier S, Bézard B, Nixon CA (2007b) The Titan 14N/15N and 12C/13C isotopic ratios in HCN from Cassini/CIRS, Icarus, 191:712–721. doi:10.1016/j.icarus.2007.06.001

Vuitton V, Yelle RV, Anicich VG (2006) The nitrogen chemistry of Titan's upper atmosphere revealed. Astrophys J 647:L175–L178

Vuitton V, Yelle RV, McEwanMJ (2007) Ion-chemistry and N-containing molecules in Titan's upper atmosphere. Icarus 191:722–742. doi:10.1016/j.icarus.2007.06.023

Vuitton V, Yelle RV, Cui J (2008) Formation and distribution of benzene on Titan. J Geophys Res, 113:E05007. doi:10.1029/2007JE002997

Waite Jr JW et al. (2005) Ion neutral mass spectrometer results from the first flyby of Titan. Science, 308:982–986

Waite JH, Young DT, Cravens TE, Coates AJ, Crary FJ, Magee B, Westlake J (2007) The process of tholin formation in Titan's upper atmosphere. Science 316:870–875. doi10.1126/science.1139727

Wilson EH, Atreya SK (2004) Current state of modeling the photochemistry of Titan's mutually dependent atmosphere and ionosphere. J Geophys Res 109:E06002. doi:10.1029/2003JE002181

Wong A-S, Morgan CG, Yung YL, Owen T (2002) Evolution of CO on Titan. Icarus 155:382–392. doi:10.1006/icar.2001.6720

Yelle RV (1991) Non-LTE models of Titan's upper atmosphere. Astrophys. J. 383:380–400

Yelle RV, Strobel DF, Lellouch E, Gautier D (1997) Engineering models for Titan's atmosphere. In: Lebreton JP (ed) HUYGENS Science, Payload and Mission, ESA SP, vol 1177, pp 243–256

Yelle RV, Cui J, Müller-Wodarg ICF (2008) Methane escape from Titan's atmosphere. J Geophys Res 113:E10003. doi:10.1029/2007JE003031

Yung YL, Allen M, Pinto JP (1984) Photochemistry of the atmosphere of Titan – comparison between model and observations. Astrophys J 55:465–506. doi:10.1086/190963